Title

On the dynamics of the eye: geodesics on a configuration manifold, motions of the gaze direction and Helmholtz's theorem

Permalink

https://escholarship.org/uc/item/56c1h7vp

Journal

Nonlinear Dynamics, 80(3)

ISSN

0924-090X

Authors

Novelia, Alyssa
O'Reilly, Oliver M

Publication Date

2015-05-01

DOI

10.1007/s11071-015-1945-0

Peer reviewed

On the Dynamics of the Eye: Geodesics on a Configuration Manifold, Motions of the Gaze Direction and Helmholtz's Theorem

Alyssa Novelia · Oliver M. O'Reilly

March 26, 2015

Abstract The simplest model with which to examine the dynamics of the human eye consists of a rigid body which is free to rotate about a fixed point. Two classical laws governing monocular vision, which are known as Listing's law and Donders' law, can be enforced in this model using a single holonomic constraint. While there has been considerable attention paid to the kinematics of the eye, the dynamics of the eye predicted by rigid body models has not received the same level of attention. In the present paper, the unforced dynamics of the resulting rigid body model are examined with particular emphasis placed on the geodesics of the configuration manifold. A comprehensive portrait of these motions is presented, and the insight gained is related to the dynamics of the gaze direction and saccadic motions of the eye. Among our results, we find that modeling the eye as an asymmetric rigid body produces a non-integrable system of governing equations and that the geodesics on the configuration manifold provide a wealth of potential motions for the gaze direction.

Alyssa Novelia
Department of Mechanical Engineering,
University of California at Berkeley,
Berkeley, CA 94720-1740
USA
Tel.: +510-642-0877
Fax: +510-643-5599
E-mail: a.novelia@berkeley.edu

Oliver M. O'Reilly
Department of Mechanical Engineering,
University of California at Berkeley,
Berkeley, CA 94720-1740
USA
Tel.: +510-642-0877
Fax: +510-643-5599
E-mail: oreilly@berkeley.edu

1 Introduction

The eye is a remarkable dynamical system capable of performing rapid coordinated movements. The groundwork on the kinematics of the eye were established by several researchers in the 1800s and synthesized and publicized in the influential treatise by Helmholtz [12] which first appeared in 1867 (see [6, 38, 45] for comprehensive historical reviews and perspectives). Helmholtz's treatise, and particularly its sections on the movement of the eye, along with the development of technologies to measure the *in vivo* rotation of the eye [34], helped fuel a renaissance in the topic in the latter part of the 20th century. Among others, experimental measurements of the saccadic motions of the eye were obtained, new insights into the ocular motor control system were found, and Listing's classical law was extended from monocular vision to binocular vision (see [6, 22]).

Concomitant with the work on kinematics, several researchers started developing models for the dynamics of the eye. These models started in the 1970s with the work of Robinson [25, 35] and has lead to models where the muscles are modeled with improved fidelity, such as [33, 43], models for a robotic eye by Cannata and Maggiali [2] and a rigid body model with generalized control torques by Ghosh *et al.* [7, 8, 31]. The resulting models can be combined with control strategies to gain a deeper understanding of how the brain controls the ocular system and enables vision.

In addition to an elaborate muscle architecture (see [5, 24]), models for the eye must accommodate Listing's law (after J. B. Listing (1808–1882)). As described by Ruete in 1853, this law states that the rotation of the eye from a specific orientation of the gaze direction (which is known as the primary position) to a current position is achieved by a rotation about an axis that is normal to the primary and current positions of the gaze direction (see Figure 1). Listing's law has several important implications for the kinematics of the eye, the most well known of which are Donders' law, Listing's half-angle rule, and Helmholtz's theorem. While these implications are discussed in Helmholtz's masterful treatise, his treatment is not easy to follow and this is partially responsible for the wide range of reviews [9, 32, 45] and alternative treatments [13, 16, 18, 20, 44] on the kinematics of the eye that have been produced.

While Helmholtz used Euler angle parameterizations of the eye's rotation, several features of the kinematics of the eye become more transparent using other parameterizations. In particular, nearly a century after Helmholtz's treatise was published, Westheimer [44] showed how parameterizations of the rotation of the eye using quaternions lead to the simplest possible representation for Listing's law. His work formed part of the foundation for Tweed, Villis and their coworkers pioneering work on measuring saccadic motions of the eye [4, 40, 41, 42]. Among the notable experimental results found by Tweed, Vilis and their coworkers, they reported in [40, p. 106] that a type of rapid movement of the eye known as a saccade could be approximated by rotations with a fixed axis and, consequently, could be considered a geodesics on the subgroup of rotations $SO(3)$ which satisfy Listing's law. In the context of eye movements, Hepp [13, 14] subsequently explored the topic of geodesics on $SO(3)$ and during the past decade Ghosh *et al.* [7, 8, 31] examined the topic of geodesics on $SO(3)$ subject to Listing's law.

Our work complements (and illuminates) the aforementioned works on geodesics by establishing new results for the motion of the gaze direction corresponding to the geodesics. We do this by leveraging an earlier work by O'Reilly and Payen [29] on rigid body motions that have constant angular velocities. For instance, we are able to show
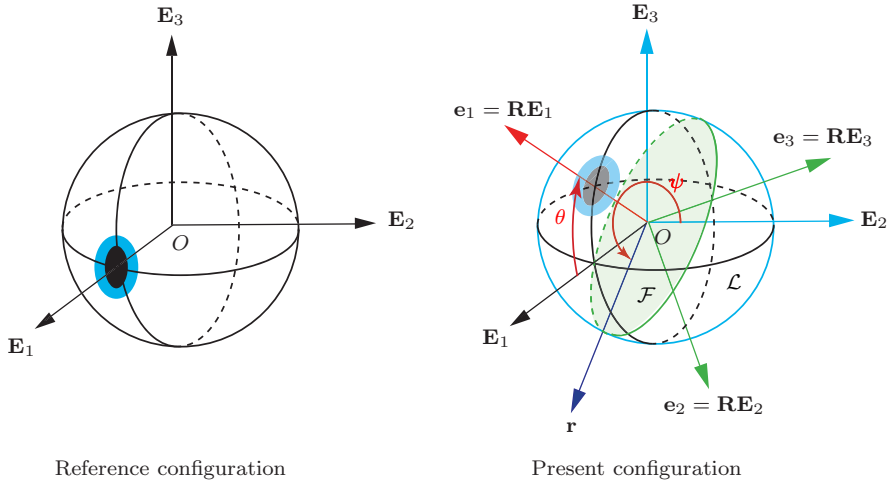
Fig. 1 *Reference configuration and present configuration of the rigid body modeling the eye where the gaze direction is assumed to be parallel to $\mathbf{e}_1$. The image of the present configuration emphasizes the observation that, following Listing's law, the axis of rotation $\mathbf{r}$ lies on the intersection of the $\mathbf{E}_2 - \mathbf{E}_3$ and $\mathbf{e}_2 - \mathbf{e}_3$ planes. The former plane is known as Listing's plane $\mathcal{L}$ and the latter is known as the focal plane $\mathcal{F}$. In ophthalmology, the reference configuration is known as the primary position and the present configuration is known as a secondary position.*

that because the geodesics for one model of the eye are motions with a fixed axis of rotation, Helmholtz's theorem [12, p. 79] and a recent work by Hess [15] can be used to establish a simple framework for saccadic motions of the eye. We also explore this framework when more elaborate models of the eye are used which don't assume that the eye is a (spherically) symmetric rigid body.

We find that the geodesic motions depend on the rigid body model for the eye. If we relax the assumption that the eye is modeled as a symmetric rigid body, then the nature of the geodesics change. Specifically, if we assume that the eye is an asymmetric rigid body, then the resulting model is non-integrable and the motions of the gaze direction corresponding to the geodesics are typically motions without a fixed axis of rotation. From the perspective of rigid body dynamics, the non-integrability of the eye model we find when the rigid body is modeled as an asymmetric rigid body is unusual. In particular, if we remove the holonomic constraint that is used to impose Listing's law, then we simply have the classical (completely integrable) problem of torque-free motion of a rigid body. Typically, when we impose a holonomic constraint that is not an explicit function of time, then we expect that the integrability of the unconstrained system will be preserved in its constrained counterpart. However, this is not the case with Listing's law.

An outline of the paper is as follows. In Section 2 of the paper, we recall representations for the rotation tensor of the eye which accommodate Listing's law and present some new perspectives of this classical law which have implications for experimental measurements (see (4) and (5) below). Listing's law is predated by a law due to Donders that pertains to the rotation of the eye about the gaze direction. Donders' law is discussed in Section 3 in a manner which completes some of the earlier numerical

results found in Helmholtz [12, p. 49] and clarifies some remarks made by Lamb [20] pertaining to the path traced by the gaze direction on the unit sphere.

Two distinct rotations feature prominently in the kinematics of the eye. The first rotation $\mathbf{R}(t)$ is the one from the primary position to the current configuration at time t and the second is the rotation $\mathbf{G}(t, t_0) = \mathbf{R}(t)\mathbf{R}^T(t_0)$ from an earlier configuration at time t_0 to the current configuration at time t. Both $\mathbf{R}(t)$ and $\mathbf{G}(t, t_0)$ have the same $\boldsymbol{\omega}$ and $\dot{\boldsymbol{\omega}}$ but not necessarily the same axis of rotation [29]. Because of Listing's law, both $\boldsymbol{\omega}(t)$ and $\dot{\boldsymbol{\omega}}(t)$ lie on a plane known as the velocity plane $\mathcal{V}(t)$. As shown in Section 4, Listing's law also has some (new) unusual implications for the components of $\boldsymbol{\omega}$ and $\dot{\boldsymbol{\omega}}$ (see (17) and (18) below). We then discuss, in Section 5, Listing's half-angle rule which states that $\mathbf{G}(t, t_0)$ has an axis of rotation that lies both on $\mathcal{V}(t)$ and $\mathcal{V}(t_0)$.

In Section 6, the equations of motion for a simple model for the eye are presented. Just as there is much to be gained by using several distinct representations for the rotation of the eye, we find it useful to use three different formulations for the equations of motion. Once these formulations have been presented we then turn to the simplest case of a symmetric model for the eye in Section 7 and show that the equations of motion are completely integrable and simplify to the case $\dot{\boldsymbol{\omega}} = \mathbf{0}$. As a result, we are able to exploit the characterization of the attitudes of constant angular velocity motions in O'Reilly and Payen [29] to obtain a complete characterization of the spherical indicatrices of the gaze direction. We find a wealth of motions of the gaze direction all of which have constant axes of rotation in the velocity plane. Motivated by the recent work of Hess [15], we also find that we can use these motions to construct arbitrary motions of the gaze direction (or saccades) provided muscle innervation is present at certain discrete events. Furthermore, an alternative proof of Helmholtz's theorem [12, p. 79] follows trivially by inspection of a phase portrait.

As discussed in Section 8, the dynamics of the eye becomes more complex when we move from the symmetric case. Indeed we find for the asymmetric rigid body model that the equations of motion are non-integrable and the motions of the gaze direction corresponding to the geodesics defy the classification possible for the symmetric case. The paper closes in Section 9 with a discussion of future applications for the results presented in this paper.

Following Gibbs, we make extensive use of tensors to represent rotations and this enables us to readily establish some classical results pertaining to the kinematics of the eye as well as to shed light on some new results. For instance, this notation enables us to easily establish the identity (A.5) that leads to additional insight into Listing's law. For ease of exposition, the reader is referred to Appendix A where relevant background on rotations and angular velocities along with quaternion and Euler angle parameterizations of rotations are presented.

2 Kinematics of the Eye and Listing's Law

We model the eye as a rigid body which is free to rotate about a point O which is fixed in the head (cf. Figure 1). A fixed reference configuration for the eye can be defined with the help of a fixed right-handed orthogonal basis $\{\mathbf{E}_1, \mathbf{E}_2, \mathbf{E}_3\}$. In this configuration the gaze direction is identified with the vector $\mathbf{E}_1$ pointing forward and $\mathbf{E}_3$ pointing vertically upwards. The vector $\mathbf{E}_2$ points to the left (right) for the left (right) eye. In the literature on the eye, the reference configuration we have described is known as the primary position.

Because the point O is fixed, the motion of the eye is purely rotational. To describe the rotation of the eye from one configuration to another, a rotation tensor is used. Thus, the rotation of the eye from the primary position to its present configuration at time t is defined by the rotation tensor $\mathbf{R}$:

$$\mathbf{e}_k = \mathbf{R}\mathbf{E}_k, \qquad (k = 1, 2, 3), \tag{1}$$

where $\{\mathbf{e}_1, \mathbf{e}_2, \mathbf{e}_3\}$ is a right-handed orthogonal basis that corotates with the eye. The rotation tensor depends both on the present configuration and the choice of reference configuration. In particular, if we change the latter, then $\mathbf{R}$ will change. Using a tensor notation for $\mathbf{R}$ highlights the dependency of $\mathbf{R}$ on the choice of $\{\mathbf{E}_1, \mathbf{E}_2, \mathbf{E}_3\}$ and also explains the emphasis on the primary position in the literature on kinematics of the eye where tensorial notations have to date not been used.

The rotation tensor $\mathbf{R}$ can be parameterized by an axis of rotation $\mathbf{r}$ and an angle of rotation θ. Equivalently, it can be parameterized by a unit quaternion $(q_0, \mathbf{q})$ where $q_0 = \cos\left(\frac{\theta}{2}\right)$ and $\mathbf{q} = \sin\left(\frac{\theta}{2}\right)\mathbf{r}$. The vector $\mathbf{e}_1$ defines the gaze direction of the eye (cf. Figure 1). It is convenient at this stage to recall that the plane spanned by $\mathbf{E}_2$ and $\mathbf{E}_3$ which passes through O is known as Listing's plane $\mathcal{L}$ and the plane spanned by $\mathbf{e}_2$ and $\mathbf{e}_3$ which passes through O is known as the focal plane $\mathcal{F}$.

Following [12, p. 48], in its original form Listing's law states that *the axis of rotation* $\mathbf{r}$ *of* $\mathbf{R}$ *is orthogonal both to the primary position* $\mathbf{E}_1$ *of the gaze direction and the position of the gaze direction* $\mathbf{e}_1 = \mathbf{R}\mathbf{E}_1$ *at time t.* That is,

$$\mathbf{r} \cdot \mathbf{E}_1 = 0 \text{ and } \mathbf{r} \cdot \mathbf{e}_1 = 0. \tag{2}$$

However, $\mathbf{r}$ is unusual in that it has the same components in both the fixed and corotational bases (cf. (A.5)) and so, in general, $\mathbf{r}$ has the representations

$$\mathbf{r} = \sum_{k=1}^{3} r_k \mathbf{E}_k = \sum_{k=1}^{3} r_k \mathbf{e}_k. \tag{3}$$

So imposing (2) and noting that $\mathbf{q} = \sin\left(\frac{\theta}{2}\right)\mathbf{r}$, we conclude that

$$\begin{aligned} \mathbf{r} &= r_2 \mathbf{E}_2 + r_3 \mathbf{E}_3 = r_2 \mathbf{e}_2 + r_3 \mathbf{e}_3, \\ \mathbf{q} &= q_2 \mathbf{E}_2 + q_3 \mathbf{E}_3 = q_2 \mathbf{e}_2 + q_3 \mathbf{e}_3. \end{aligned} \tag{4}$$

Thus, as a consequence of (3), Listing's law can be expressed in a variety of equivalent manners featuring one component of either $\mathbf{r}$ or $\mathbf{q}$:

$$\mathbf{q} \cdot \mathbf{E}_1 = 0, \text{ or } \mathbf{r} \cdot \mathbf{E}_1 = 0, \text{ or } \mathbf{q} \cdot \mathbf{e}_1 = 0, \text{ or } \mathbf{r} \cdot \mathbf{e}_1 = 0. \tag{5}$$

From a geometrical perspective, we can also immediately conclude that the axis of rotation of $\mathbf{R}$ lies on the line of intersection of the focal plane and Listing's plane (cf. Figure 1). We also note that the identities (3) have relevance to several experimental works on eye movements where the components $\theta \mathbf{r} \cdot \mathbf{E}_k$ of the rotation vector as in Hess [15], or $\mathbf{q} \cdot \mathbf{E}_k$, as in Tweed *et al.* [40], are presented.

We now follow Westheimer [44] and examine the quaternion parameterization of a rotation $\mathbf{R}$ which satisfies Listing's law (5). To proceed we use (A.2) and (A.6), and
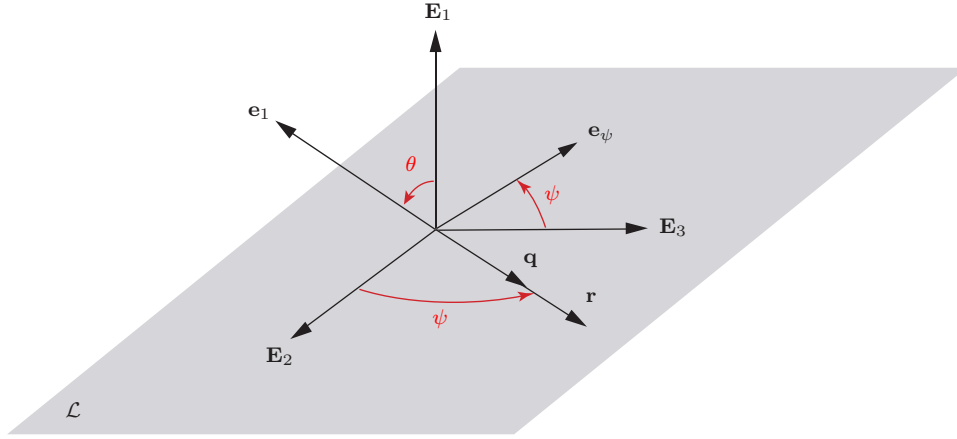
Fig. 2 *Schematic showing Listing's plane $\mathcal{L}$ and the angles ψ and θ which can be used to parameterize $\mathbf{R}$. Both sets of orthonormal vectors $\{\mathbf{E}_2, \mathbf{E}_3\}$ and $\{\mathbf{r}, \mathbf{e}_\psi\}$ span $\mathcal{L}$.*

find that it is prudent to introduce a second angle ψ in addition to the angle of rotation θ:[1]

$$q_0 = \cos\left(\frac{\theta}{2}\right),$$

$$q_1 = 0,$$

$$q_2 = \sin\left(\frac{\theta}{2}\right)\cos(\psi),$$

$$q_3 = \sin\left(\frac{\theta}{2}\right)\sin(\psi). \tag{6}$$

This is the most general representation for $(q_0, \mathbf{q})$ that is compatible with Listing's law.

Referring to Figure 2, in order to provide additional insight into the angles ψ and θ, it is convenient to define a vector $\mathbf{e}_\psi$ which lies in Listing's plane and is normal to $\mathbf{r}$:

$$\mathbf{r} = \cos\left(\psi\right)\mathbf{E}_2 + \sin\left(\psi\right)\mathbf{E}_3, \qquad \mathbf{e}_\psi = \cos\left(\psi\right)\mathbf{E}_3 - \sin\left(\psi\right)\mathbf{E}_2. \tag{7}$$

Substituting for $(q_0, \mathbf{q})$ from (6) into (A.6), representations for the components R_{ik} of $\mathbf{R}$ can be found. Three of these components can then be used to examine the parameterization of the path of the gaze direction $\mathbf{e}_1(t)$:

$$\begin{aligned} \mathbf{e}_1 &= \cos\left(\theta\right)\mathbf{E}_1 - \sin\left(\theta\right)\mathbf{e}_\psi \\ &= \cos\left(\theta\right)\mathbf{E}_1 + \sin\left(\theta\right)\left(\cos\left(\psi - \frac{\pi}{2}\right)\mathbf{E}_2 + \sin\left(\psi - \frac{\pi}{2}\right)\mathbf{E}_3\right). \end{aligned} \tag{8}$$

---

[1] In his seminal paper Westheimer [44] uses the angles c and ω to parameterize the quaternion. The correspondence between his notation and ours is as follows: $\omega = \theta$, $\sin(c) = \cos(\psi)$ and $\cos(c) = \sin(\psi)$. We note for completeness that in the notation of Tweed and Vilis and their coworkers [4, 40, 41, 42]: $q_V = \mathbf{q} \cdot \mathbf{E}_2$, $q_H = \mathbf{q} \cdot \mathbf{E}_3$, and $q_T = \mathbf{q} \cdot \mathbf{E}_1$.

When the unit vector $\mathbf{e}_1$ is expressed in the second manner shown above it becomes apparent that θ is the colatitude and $\psi - \frac{\pi}{2}$ is the azimutal coordinate for the spherical locus of $\mathbf{e}_1$ (cf. Figure 1). We also note that

$$\mathbf{E}_1 \times \mathbf{e}_1 = \sin(\theta) \, \mathbf{r}. \tag{9}$$

Because $\mathbf{E}_1$ is normal to Listing's plane and $\mathbf{e}_1$ is normal to the focal plane, the result that $\mathbf{E}_1 \times \mathbf{e}_1 = \sin(\theta) \, \mathbf{r}$ can be considered as an alternative proof that the axis of rotation $\mathbf{r}$ lies on the intersection of Listing's plane and the focal plane.

It is convenient to establish expressions for $\mathbf{e}_i$ in terms of the angles θ and ψ that were used to parameterize q_0 and $\mathbf{q}$. Substituting (6) into (A.6) and collecting terms, we find the following illuminating representation:

$$\begin{bmatrix} \mathbf{e}_1 \\ \mathbf{e}_2 \\ \mathbf{e}_3 \end{bmatrix} = \begin{bmatrix} 1 & 0 & 0 \\ 0 & \cos(\nu) & -\sin(\nu) \\ 0 & \sin(\nu) & \cos(\nu) \end{bmatrix} \begin{bmatrix} \cos(\theta) & 0 & -\sin(\theta) \\ 0 & 1 & 0 \\ \sin(\theta) & 0 & \cos(\theta) \end{bmatrix} \begin{bmatrix} 1 & 0 & 0 \\ 0 & \cos(\nu) & \sin(\nu) \\ 0 & -\sin(\nu) & \cos(\nu) \end{bmatrix} \begin{bmatrix} \mathbf{E}_1 \\ \mathbf{E}_2 \\ \mathbf{E}_3 \end{bmatrix}, \tag{10}$$

where

$$\nu = \psi - \frac{\pi}{2}. \tag{11}$$

This representation enables an easy comparison of the quaternion representation featuring θ and ψ and an Euler angle representation.

2.1 Representation of Listing's Law in terms of a 1-2-1 Euler Angle Parameterization

The rotation tensor can also be parameterized using a set of 1-2-1 Euler angles: $\theta_1, \theta_2, \theta_3$. Details on this set of angles can be found in Appendix A. With the assistance of $(A.9)_2$, we find an expression for $q_1 = \mathbf{q} \cdot \mathbf{e}_1 = \mathbf{q} \cdot \mathbf{E}_1$ in terms of this set of Euler angles:

$$q_1 = \cos\left(\frac{\theta_2}{2}\right) \sin\left(\frac{\theta_1}{2} + \frac{\theta_3}{2}\right). \tag{12}$$

Now Listing's law implies that $q_1 = 0$. So, after considering the ranges of the two Euler angles θ_1 and θ_2, one finds that Listing's law can be expressed in a simple form (equivalent to the one found in Helmholtz [12, p. 75, Eq. (2a)]):

$$\theta_1 + \theta_3 = 0. \tag{13}$$

Thus given any gaze direction (defined by $\theta_{1,2}$ (cf. (A.8)) there is a unique given angle $\theta_3 = -\theta_1$. It is easy to see from (10) that the condition $\theta_3 = -\theta_1$ is identical to (11). Indeed we can identify ψ and θ with the Euler angles θ_1 and θ_2 respectively, provided θ is restricted to range from 0 to π.

3 Listing's Law implies Donders' Law

Torsion of the eye, or ocular torsion, is the rotation of the eye about the direction of gaze (i.e., the $\mathbf{e}_1$ axis). Measuring this rotation is challenging [17, 19] and, just as in the development of theories for deformable elastic rods (cf. [1, 10, 23]), the term "torsion" can be confusing. From a historical perspective it is interesting to note that this confusion both in continuum mechanics and ophthalmology can be traced to the

(a)

(b)
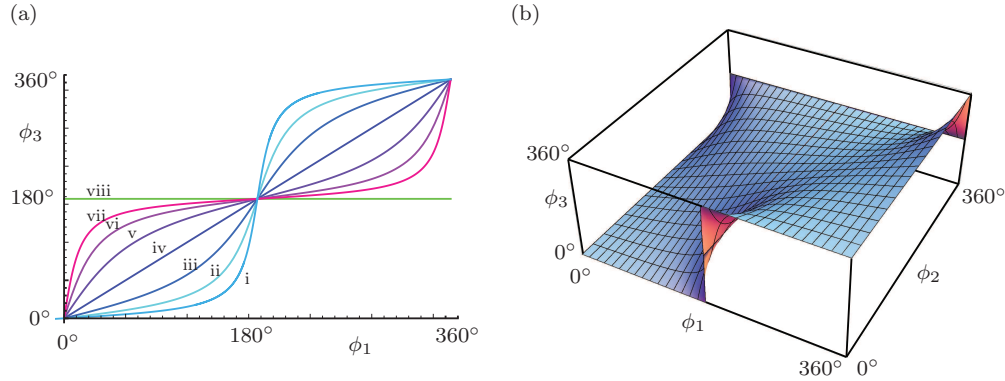
Fig. 3 *Representations of the solution ϕ_3 of the (14) as a function of the Euler angles ϕ_1 and ϕ_2. The figure shows that given an orientation of the gaze direction then a corollary of Listing's law implies that there is a unique value of ϕ_3. In (a): i: $\phi_2 = \pi/16$, ii: $\phi_2 = \pi/8$, iii: $\phi_2 = \pi/4$, iv: $\phi_2 = \pi/2$, v: $\phi_2 = 3\pi/4$, vi: $\phi_2 = 7\pi/8$, vii: $\phi_2 = 15\pi/16$, and viii $\phi_2 = \pi$.*

early part of the 19th century when applications of the differential geometry of space curves and the parameterizations of rotations were starting to multiply.

Donders' law pertains to torsion of the eye and can be stated as follows *for every orientation of the line of sight, there is a unique orientation of the eye*. In other words, if the line of sight (fixation/gaze) $\mathbf{e}_1$ is known, then so too are $\mathbf{e}_2$ and $\mathbf{e}_3$. This law predates Listing's law and it is not immediately apparent how motions which satisfy Listing's law can also satisfy Donders' law. For example, following Lamb [20], consider a motion where the gaze direction $\mathbf{e}_1$ describes a closed path on the sphere and returns to its original orientation. If $\mathbf{e}_2$ (or equivalently $\mathbf{e}_3$) does not return to its original orientation, then the motion of the eye is in violation of Donders' law. However, examining all possible motions of the eye compatible with Listing's law and computing this net rotation is prohibitive.[2] Instead, we follow (and provide additional insight and results into) a straightforward approach that follows Helmholtz [12] who used a set of 3-2-1 Euler angles to parameterize the rotation of the eye. With this parameterization, the gaze direction is uniquely prescribed by the first two angles ϕ_1 and ϕ_2. The third angle, ϕ_3 can then be used to describe the relative rotation of $\mathbf{e}_2$ and $\mathbf{e}_3$ about $\mathbf{e}_1$ [27]. In other words, the angle ϕ_3 describes ocular torsion (or as it is sometimes known rolling movement of the eye because the iris appears to roll on the sclera). If a motion of the eye is in agreement with Donders' law, then for each pair of values (ϕ_1, ϕ_2), there corresponds a single value of ϕ_3. In this case, the net rotation about $\mathbf{e}_1$ (i.e., the change in ϕ_3) during a motion where this vector describes a closed path on the sphere and returns to its original orientation is zero.

The representation of Listing's law using the 3-2-1 set of Euler angles is not as transparent as that provided by a 1-2-1 set of Euler angles. To start, we impose Listing's law by setting $q_1 = 0$ in (A.11) and then invoke multiple trigonometric identities to

---

[2] The techniques needed to examine such a relative rotation are identical to those used to examine total twist in rods and also involve geometric phases [1,10,23,27].

find the known result:[3]

$$\tan\left(\phi_3\right) = \frac{\sin\left(\phi_1\right)\sin\left(\phi_2\right)}{\cos\left(\phi_1\right) + \cos\left(\phi_2\right)}. \tag{14}$$

That is, Listing's law is equivalent to the statement that the 3-2-1 set of Euler angles are related by (14). Motions of the gaze direction where $\phi_1 = 0$ or $\phi_2 = 0$ are known as tertiary motions. For these motions, the gaze direction either moves up and down or from left to right, and we can easily see from (14) that $\phi_3 = 0$. For other motions, we need to solve (14) numerically to find the value of ϕ_3 for a given pair ϕ_1 and ϕ_2 that is compatible with Listing's law. These numerical results are shown in Figure 3, and they show that for each pair ϕ_1 and ϕ_2, and consequently, each orientation of the gaze direction, there is a unique value of ϕ_3 compatible with (14).[4] The results shown in Figure 3 also illuminate why the angle ϕ_3 is sometimes known as "false torsion" (cf. [26, p. 547]): for most orientations of the gaze direction $\phi_3 \neq 0$. On the basis of the numerical results shown in Figure 3, we conclude (the known result) that Donders' law is a consequence of Listing's law.
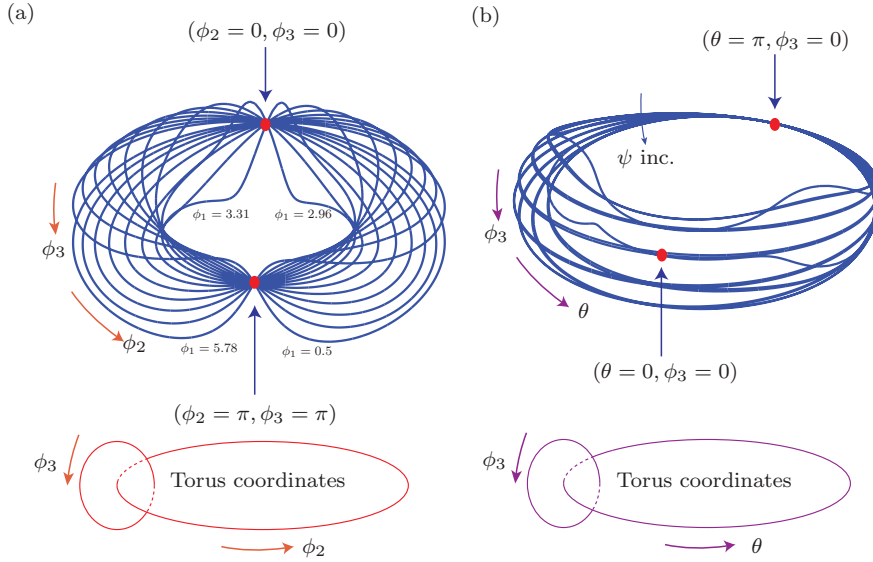
Fig. 4 *Representations on a torus of (a) the solution ϕ_3 of the (14) as a function of the Euler angles ϕ_1 and ϕ_2 and (b) the solution ϕ_3 of (16) as a function of the angles θ and ψ. In (a) ϕ_1 is increased from 0.5 to $2\pi - 0.5$ and, for a given ϕ_2 value, (14) is solved for ϕ_3, and in (b) ψ is increased from 0.5 to $2\pi - 0.5$ and, for a given θ value, (16) is solved for ϕ_3.*

The conclusion that Donders' law is a corollary to Listing's law can also be found using the parameterization featuring ψ and θ and the 1-2-1 Euler angle parameterization. We restrict attention to the former parameterization and find that in order to

---

[3] The identity (14) is equivalent to one found in [12, p. 49] and [26, Eqn. (a)]. In the literature (cf., e.g., [45]) it is often linearized (about the primary position) to the equation that is equivalent to $\phi_3 = \frac{1}{2}\phi_2\phi_1$.

[4] The data shown in Figure 3 completes the tables of results for a limited set of discrete values of ϕ_1 and ϕ_2 presented in [12, p. 49].

compute an expression for ϕ_3 as a function of θ and ψ, it is convenient to first note that

$$\tan(\phi_3) = \frac{R_{32}}{R_{33}} = \frac{2q_2 q_3}{2q_0^2 + 2q_3^2 - 1}. \tag{15}$$

To establish (15), we used the representation (A.6) for $\mathbf{R}$ and then compared the components to the corresponding representation of $\mathbf{R}$ using a 3-2-1 set of Euler angles that were discussed in Section A.2.2. Using the expressions (6) for the quaternion components which are compatible with Listing's law, it follows that (15) implies

$$\tan(\phi_3) = \frac{\sin(2\psi)\sin^2\left(\frac{\theta}{2}\right)}{\cos(\theta) + 2\sin^2(\psi)\sin^2\left(\frac{\theta}{2}\right)}. \tag{16}$$

While the function $\phi_3(\psi,\theta)$ provided by (16) can be presented in a manner similar to that shown in Figure 3, in the interests of brevity we refrain from doing so here. Such numerical results would also enable us to conclude that Donders' law follows from Listing's law.

One issue that is potentially misleading about Figure 3 is the values of ϕ_2 and ϕ_3 at the endpoints of the graph. To see that this is an artifact of the coordinate system and doesn't imply that motions of the eye exist where $\mathbf{e}_1$ returns to its original orientation and $\mathbf{e}_2$ and $\mathbf{e}_3$ have rotated through $360°$ about $\mathbf{e}_1$ during the motion, it is necessary to display Figure 3 in a different manner. First, we note that ϕ_2 and ϕ_3 range from 0 to 2π and so these coordinates define a torus. We now proceed to plot the level sets shown in Figure 3(a) on a torus. The resulting construction is shown in Figure 4(a). From this figure, we observe that when $\mathbf{e}_1$ returns to its original orientation, there is no net relative rotation of $\mathbf{e}_2$ and $\mathbf{e}_3$ about $\mathbf{e}_1$. As shown in Figure 4(b), this conclusion can be inferred by performing the same construction with the solutions to (16) where now the torus is parameterized by θ and ψ.

4 Listing's Law, Angular Velocity and Angular Acceleration

Rotations which satisfy Listing's law have several other interesting features particularly with respect to the angular velocity vector $\boldsymbol{\omega}$. First, if Listing's law in the form $q_1 = 0$ (and $\dot{q}_1 = 0$) is imposed, then it is easy to see from (A.13) and (A.14) that two components of the angular velocity vector expressed in the reference and corotational bases are identical while the third are equal and opposite:

$$\begin{aligned}
\boldsymbol{\omega} \cdot \mathbf{E}_1 &= -\boldsymbol{\omega} \cdot \mathbf{e}_1 = 2(\dot{q}_3 q_2 - \dot{q}_2 q_3), \\
\boldsymbol{\omega} \cdot \mathbf{E}_2 &= \boldsymbol{\omega} \cdot \mathbf{e}_2 = 2(\dot{q}_2 q_0 - \dot{q}_0 q_2), \\
\boldsymbol{\omega} \cdot \mathbf{E}_3 &= \boldsymbol{\omega} \cdot \mathbf{e}_3 = 2(\dot{q}_3 q_0 - \dot{q}_0 q_3).
\end{aligned} \tag{17}$$

While the components of $\boldsymbol{\omega}$ in the fixed and corotational basis are related by $\mathbf{R}$, $\boldsymbol{\omega}\cdot\mathbf{E}_k = (\mathbf{R}\boldsymbol{\omega})\cdot\mathbf{e}_k$, these relationships don't typically simplify to (17). In addition, (17) and the identities $\dot{\mathbf{e}}_i = \boldsymbol{\omega} \times \mathbf{e}_i$ imply that the components of the angular acceleration vector $\dot{\boldsymbol{\omega}}$ satisfy the identities

$$\dot{\boldsymbol{\omega}} \cdot \mathbf{E}_1 = -\dot{\boldsymbol{\omega}} \cdot \mathbf{e}_1, \qquad \dot{\boldsymbol{\omega}} \cdot \mathbf{E}_2 = \dot{\boldsymbol{\omega}} \cdot \mathbf{e}_2, \qquad \dot{\boldsymbol{\omega}} \cdot \mathbf{E}_3 = \dot{\boldsymbol{\omega}} \cdot \mathbf{e}_3. \tag{18}$$

The relationships (17) and (18) are atypical and are a consequence of Listing's constraint.

The identities (17), which have not appeared previously in the literature on Listing's law, have consequences for measurements of the eye's angular velocity. If angular rate sensors are used that are fixed to the head, and consequently measure $\boldsymbol{\omega} \cdot \mathbf{E}_i$, then these measurements are readily translated into the more difficult to measure $\boldsymbol{\omega} \cdot \mathbf{e}_i$ without having to determine $\mathbf{e}_i(t)$.[5] We also take this opportunity to emphasize that (17) demonstrates that although the axis of rotation of $\mathbf{R}$ lies in Listing's plane, $\boldsymbol{\omega}$ doesn't necessarily lie in the same plane.

4.1 A Representation for the Angular Velocity Vector

Before turning to examining the representation for $\boldsymbol{\omega}$ featuring the angles ψ and θ in (6), it is convenient to use these angles and define a basis for $\mathbb{E}^3$ composed of the vectors $\mathbf{w}_1 = \mathbf{r}$, $\mathbf{w}_2$ and $\mathbf{w}^3$:

$$
\begin{aligned}
\mathbf{w}_1 &= \mathbf{r} = \cos(\psi)\mathbf{E}_2 + \sin(\psi)\mathbf{E}_3, \\
\mathbf{w}_2 &= \mathbf{E}_1 - \mathbf{e}_1 = \left(1 - \cos(\theta)\right)\mathbf{E}_1 + \sin(\theta)\mathbf{e}_\psi, \\
\mathbf{w}^3 &= \mathbf{w}_1 \times \mathbf{w}_2 = \sin(\theta)\mathbf{E}_1 - \left(1 - \cos(\theta)\right)\mathbf{e}_\psi.
\end{aligned}
\tag{19}
$$

The following inverse relations can be found using (19):

$$
\begin{bmatrix} \mathbf{E}_1 \\ \mathbf{e}_\psi \end{bmatrix} = \frac{1}{2} \begin{bmatrix} 1 & \cot\left(\frac{\theta}{2}\right) \\ \cot\left(\frac{\theta}{2}\right) & -1 \end{bmatrix} \begin{bmatrix} \mathbf{w}_2 \\ \mathbf{w}^3 \end{bmatrix}.
\tag{20}
$$

When $\theta \neq 0$, the vectors $\left\{\mathbf{w}_1, \mathbf{w}_2, \mathbf{w}^3\right\}$ form an orthogonal basis for $\mathbb{E}^3$ where $\|\mathbf{w}_2\| = \|\mathbf{w}^3\| = 2\sin\left(\frac{\theta}{2}\right)$ and $\|\mathbf{w}_1\| = 1$.
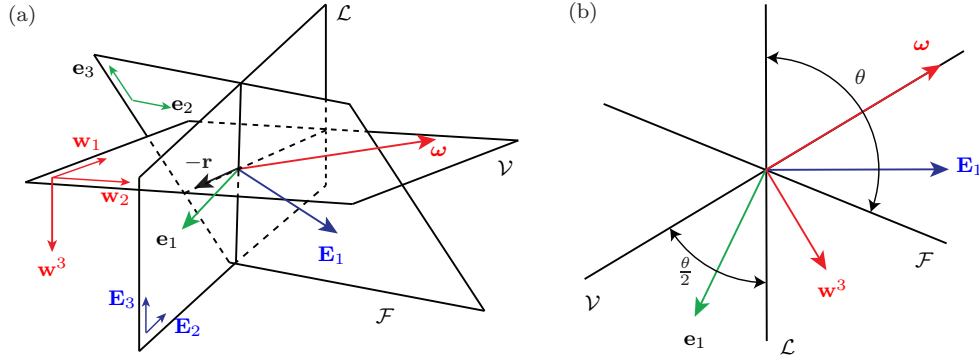
Fig. 5 *(a) The focal plane $\mathcal{F}$, Listing's plane $\mathcal{L}$, and the displacement (velocity) plane $\mathcal{V}$ for a given gaze direction $\mathbf{e}_1$ and primary direction $\mathbf{E}_1$. (b) A side view of the three planes taken along the axis of rotation $\mathbf{r}$ which lies at the intersection of the planes $\mathcal{F}$, $\mathcal{L}$ and $\mathcal{V}$.*

Using the quaternion parameterization (6) featuring ψ and θ that is compatible with Listing's law we can compute a representation to $\boldsymbol{\omega}$ that is equivalent to (17).

---

[5] Examples of such results can be seen in [42, Figure 2].

With the help of (19), the resulting representation has a compact and illuminating form:

$$\boldsymbol{\omega} = \dot{\theta}\mathbf{w}_1 + \dot{\psi}\mathbf{w}_2. \tag{21}$$

As anticipated, the term featuring $\dot{\theta}$ is parallel to the axis of rotation, and, so if $\dot{\psi} = 0$, then $\boldsymbol{\omega}$ will be parallel to $\mathbf{r}$.

The plane through the origin that is spanned by $\mathbf{w}_1$ and $\mathbf{w}_2$ is known as the velocity plane $\mathcal{V}$ (cf. [45] and Figure 5).[6] By construction the unit normal $\mathbf{n}$ to $\mathcal{V}$ is parallel to $\mathbf{w}^3$:[7]

$$\mathbf{n} = \frac{\mathbf{w}^3}{\|\mathbf{w}^3\|} = \cos\left(\frac{\theta}{2}\right)\mathbf{E}_1 - \sin\left(\frac{\theta}{2}\right)\mathbf{e}_\psi$$
$$= q_0\mathbf{E}_1 - q_2\mathbf{E}_3 + q_3\mathbf{E}_2. \tag{22}$$

Noting the representations, from (8) and $(19)_3$,

$$\mathbf{e}_1 = \cos\left(\theta\right)\mathbf{E}_1 - \sin\left(\theta\right)\mathbf{e}_\psi,$$
$$\mathbf{w}^3 = 2\sin\left(\frac{\theta}{2}\right)\left(\cos\left(\frac{\theta}{2}\right)\mathbf{E}_1 - \sin\left(\frac{\theta}{2}\right)\mathbf{e}_\psi\right), \tag{23}$$

it follows that $\mathbf{w}^3$ lies on the plane formed by $\mathbf{e}_1$ and $\mathbf{E}_1$ and that $\mathbf{w}^3$ bisects this pair of vectors:[8]

$$\mathbf{n} \cdot \mathbf{E}_1 = \cos\left(\frac{\theta}{2}\right), \qquad \mathbf{n} \cdot \mathbf{e}_1 = \cos\left(\frac{\theta}{2}\right). \tag{24}$$

Representative examples of these geometric features of $\mathbf{w}^3$ can be seen in Figures 5 and 6(a).

4.2 Listing's Constraint

We observe from (21) that the angular velocity vector satisfies the condition

$$\boldsymbol{\omega} \cdot \mathbf{n} = 0, \tag{25}$$

where the normal vector $\mathbf{n}$ is defined by (22). The equation (25) is known as Listing's constraint: it is the restriction that $\boldsymbol{\omega}$ lies on the plane $\mathcal{V}$ which ensures that the axis of rotation $\mathbf{r}$ remains on Listing's plane, or equivalently, the focal plane. Interestingly, the normal vector in Listing's constraint is the normal vector to $\mathcal{V}$ rather than $\mathcal{L}$. Listing's constraint (25) is integrable (holonomic) and restricts the rotation tensor $\mathbf{R}$ to lie in a submanifold of $SO(3)$. As discussed in [7,31], this submanifold is the real projective plane $\mathbb{RP}^2$.

---

[6] The plane $\mathcal{V}$ is denoted by P_ω in [2,7] and is known as the displacement plane in the works by Tweed, Villis *et al.* [40,41,42] who credit the discovery of the plane to Helmholtz [12]. Tweed *et al.*'s papers contain experimental evidence for the existence of $\mathcal{V}$. The basis set $\left\{\mathbf{w}_1, \mathbf{w}_2, \mathbf{w}^3\right\}$ that we are using is novel.

[7] In the classical literature, the vector $\mathbf{n}$ is parallel to what Helmholtz [12, p. 78] refers to as the "temporal atropic line."

[8] The angle $\frac{\theta}{2}$ between $\mathcal{V}$ and Listing's plane $\mathcal{L}$ can be verified by comparing the angle between the respective normal vectors $\mathbf{n}$ and $\mathbf{E}_1$ to these planes.

(a)   (b)
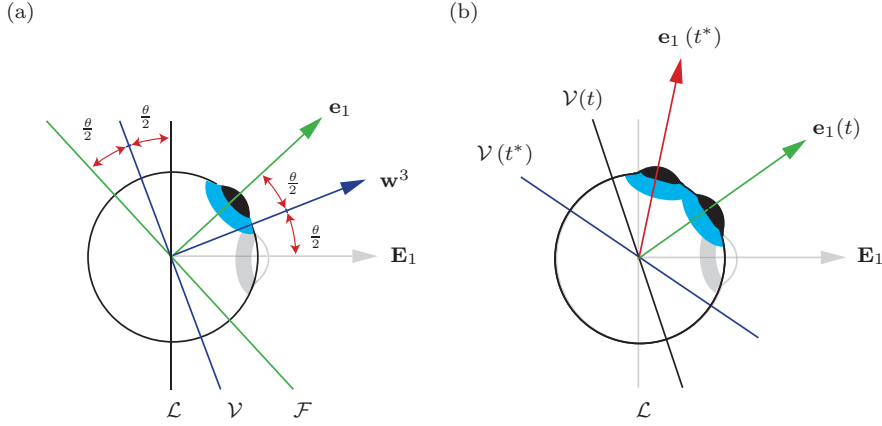
Fig. 6 *Configurations of the eye and the gaze direction. (a) Secondary position of the eye showing Listing's plane $\mathcal{L}$, the focal plane $\mathcal{F}$, and the velocity plane $\mathcal{V}$. (b) Two secondary positions of the eye and their respective velocity planes $\mathcal{V}(t)$ and $\mathcal{V}(t^*)$.*

4.3 Another Representation for the Angular Acceleration Vector

With the future goal of examining the dynamics of the eye, it is of interest to compute the angular acceleration $\dot{\boldsymbol{\omega}}$. Earlier in (18) we observed that this vector's components in the fixed and corotational bases were simply related. An additional useful representation can be found using the basis vectors $\{\mathbf{w}_1, \mathbf{w}_2, \mathbf{w}^3\}$. A direct differentiation of (21) leads to the representation

$$\dot{\boldsymbol{\omega}} = \left(\ddot{\theta} + \dot{\psi}\sin(\theta)\right)\mathbf{w}_1 + \left(\ddot{\psi} + \dot{\psi}\dot{\theta}\cot\left(\frac{\theta}{2}\right)\right)\mathbf{w}_2. \tag{26}$$

The fact that $\dot{\boldsymbol{\omega}}$ is coplanar with $\boldsymbol{\omega}$ and lies in the velocity plane $\mathcal{V}$ was recently noticed by Cannata and Maggiali [2]. This result has significant implications for the dynamics of the eye and the constraint moment $\mathbf{M}_c$ required to enforce Listing's law.

5 Listing's Half-Angle Rule

Listing's law in its original form pertains to the rotation of the gaze direction from its primary position to its current position. In practice, it is far more useful to have a version of this law which describes the rotation of the eye between two non-primary configurations. The resulting law is known as Listing's half-angle rule and, among others, is notably discussed in the works by Helmholtz [12, p. 77] and Tweed *et al.* [40, 42]. Because of our forthcoming works on geodesic motions, we find it convenient to discuss the half-angle rule as well as to present an alternative proof.

Suppose the gaze direction $\mathbf{e}_1(t)$ has a given orientation described by a rotation $\mathbf{R}(t)$ and we wish to consider a motion of the eye from this secondary position to another position, say $\mathbf{e}_1(t^*)$ (cf. Figures 6(b) and 7). One method to compute the resulting rotation is to subject the eye to the inverse rotation $\mathbf{R}^T(t)$ (so $\mathbf{e}_1(t)$ is aligned
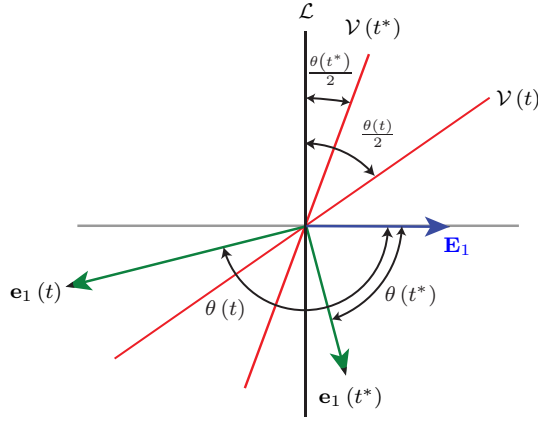
Fig. 7 *Schematic showing the displacement planes $\mathcal{V}(t)$ and $\mathcal{V}(t^*)$ corresponding to two distinct orientations of the gaze direction. The viewpoint for this figure is such that the axis of rotation corresponding to the motion from $\mathbf{e}_1(t)$ to $\mathbf{e}_1(t^*)$ is perpendicular to the plane of the figure.*

with its primary position $\mathbf{E}_1$) and then subject the eye to a rotation $\mathbf{R}(t^*)$ which will transform $\mathbf{E}_1$ to $\mathbf{e}_1(t^*)$. Alternatively, we can subject the eye to the compound rotation

$$\mathbf{G}\left(t^*,t\right) = \mathbf{R}\left(t^*\right)\mathbf{R}^T(t). \tag{27}$$

Both of the rotations $\mathbf{R}(t^*)$ and $\mathbf{R}(t)$ satisfy Listing's law, so it is natural to ask if anything can be said about the compound rotation $\mathbf{G}(t^*,t)$? The answer is yes. First, it can be shown that the axis of rotation of $\mathbf{G}(t^*,t)$ lies on the velocity plane $\mathcal{V}(t)$ associated with the rotation $\mathbf{R}(t)$ (see Figure 6(b)). Because this plane bisects $\mathbf{E}_1$ and $\mathbf{e}_1(t)$, this law is known in the literature as Listing's half-angle rule.

As regards proofs of Listing's half-angle rule, a terse descriptive proof is given on page 77 in Helmholtz's treatise [12], Lamb [20] provides a proof based on spherical geometry, Tweed *et al.* [40] present an alternative proof based on Clifford algebras and a fourth proof is presented in Judge [18] based on the observation that any rotation can be decomposed into the product of two reflections. Here, we present yet another proof which also serves to show that the axis of rotation of $\mathbf{G}(t^*,t)$ lies in the intersection of the velocity planes associated with $\mathbf{R}(t)$ and $\mathbf{R}(t^*)$. Our proof can also be viewed as an elaboration of that provided by Helmholtz.

Consider two orientations $\mathbf{R}(t)$ and $\mathbf{R}(t^*)$ of the eye and suppose that the angles and quaternions associated with these orientations are denoted by $(\psi(t), \theta(t), q_0(t), \mathbf{q}(t))$ and $(\psi(t^*), \theta(t^*), q_0(t^*), \mathbf{q}(t^*))$, respectively. The quaternion $(p_0, \mathbf{p})$ associated with the rotation $\mathbf{G}(t^*,t) = \mathbf{R}(t^*)\mathbf{R}^T(t)$ can be determined using a well-known formulae due to Rodrigues:

$$p_0 = q_0(t)q\left(t^*\right) + \mathbf{q}(t)\cdot\mathbf{q}\left(t^*\right), \qquad \mathbf{p} = q_0(t)\mathbf{q}\left(t^*\right) + q_0\left(t^*\right)\mathbf{q}(t) + \mathbf{q}(t)\times\mathbf{q}\left(t^*\right). \tag{28}$$

The axis $\mathbf{c}$ and angle β of the rotation $\mathbf{G}(t^*,t)$ can be found from the identifications $p_0 = \cos\left(\frac{\beta}{2}\right)$ and $\mathbf{p} = \sin\left(\frac{\beta}{2}\right)\mathbf{c}$ but these are not of interest here.

It suffices for the present purposes to examine the direction of $\mathbf{c}$ and to show that it lies in the velocity plane associated with the rotation $\mathbf{R}(t)$. The velocity plane $\mathcal{V}(t)$ associated with $\mathbf{R}(t)$ has a normal vector $\mathbf{w}^3(t)$ defined by (19). As $\beta \neq 0$, we can compute $\mathbf{p} \cdot \mathbf{w}^3(t)$:

$$\mathbf{p} \cdot \mathbf{w}^3(t) = \left(q_0(t)\mathbf{q}\left(t^*\right) + q_0\left(t^*\right)\mathbf{q}(t) + \mathbf{q}(t) \times \mathbf{q}\left(t^*\right) \right) \cdot \mathbf{w}^3(t). \tag{29}$$

Because $\mathbf{w}^3(t) = \mathbf{w}_1(t) \times \mathbf{w}_2(t)$ and $\mathbf{w}_1(t) \parallel \mathbf{q}(t)$, we find that the above expression simplifies dramatically:

$$\mathbf{p} \cdot \mathbf{w}^3(t) = \mathbf{q}\left(t^*\right) \cdot \left(4\cos^2\left(\frac{\theta(t)}{2}\right)\sin\left(\frac{\theta(t)}{2}\right)\mathbf{E}_1 \right). \tag{30}$$

However, from Listing's law $\mathbf{q}\left(t^*\right) \cdot \mathbf{E}_1 = 0$, and so we conclude that the axis of rotation of the compound rotation $\mathbf{G}\left(t^*, t\right)$ lies in the velocity plane $\mathcal{V}(t)$ associated with $\mathbf{R}(t)$. This result is Listing's half-angle rule in the work by Tweed, Vilis and their coworkers (see, e.g., [40, 42, 45]).

The rule actually features two velocity planes. One method of seeing this is to compute $\mathbf{p} \cdot \mathbf{w}^3\left(t^*\right)$. Paralleling (29) and (30), we find that $\mathbf{p} \cdot \mathbf{w}^3\left(t^*\right) = 0$. Hence, we can conclude that, in addition to $\mathbf{p}$ lying on $\mathcal{V}(t)$, $\mathbf{p}$ also lies on $\mathcal{V}(t^*)$. Our third observation about $\mathbf{p}$ is that it is also the axis of rotation of the inverse rotation

$$\mathbf{G}\left(t, t^*\right) = \mathbf{G}^T\left(t^*, t\right) = \mathbf{R}(t)\mathbf{R}^T\left(t^*\right). \tag{31}$$

In conclusion, given two orientations of the eye, the axis of rotation of the rotation taking one to the other and vice-versa lies on the intersection of the velocity planes associated with the pair of orientations. This is the form of Listing's half-angle rule that can be found in Helmholtz's treatise [12].

6 A Simple Dynamic Model

The human eye is widely modeled as a rigid body which is free to rotate about a point O which is fixed in the head and a wide range of models for the eye appear in the literature (see, e.g., [2, 8, 33, 43]) with the state-of-the-art dynamic model appearing in the recent work of Wei *et al.* [43]. The model in [43] is unique in its modeling of the complex system of six muscle groups acting on the eye. Among other issues these models are designed to help further ongoing research on the neuromuscular scheme which controls vision. Here, with the goal of advancing fundamental understanding of the dynamics of the eye, we provide a detailed examination of its unforced dynamics.

6.1 Constraint Moment

To proceed, we model the eye as a rigid body with an inertia tensor $\mathbf{J}$. We assume that the basis vectors $\mathbf{e}_k$ are parallel to the principal axes of $\mathbf{J}$ with corresponding mass moments of inertia λ_k where $k = 1, 2, 3$. Because the motion of the eye is assumed to obey Listing's law, the eye is subject to a constraint moment $\mathbf{M}_c$ which enforces

Listing's constraint (25). We follow standard practice and prescribe this constraint moment as[9]

$$\mathbf{M}_c = \mu\mathbf{n}, \tag{32}$$

where μ is a Lagrange multiplier.

6.2 Formulations of the Equations of Motion

Several alternative formulations of the equations of motion for the rigid body model for the eye are available and to obtain distinct insights it is convenient for our purposes to use three different formulations. In each of the three formulations, we ignore the applied moments due to the muscle groups and soft connective tissues and assume that the sole moment acting on the eye is the constraint moment $\mathbf{M}_c$.

The first formulation we use is based on a balance of angular momentum relative to the center of mass O of the eye:

$$\mathbf{J}\dot{\boldsymbol{\omega}} + \boldsymbol{\omega} \times (\mathbf{J}\boldsymbol{\omega}) = \mathbf{M}_c. \tag{33}$$

If $\mathbf{J} \neq \lambda\mathbf{I}$, then μ will generally not be zero and external intervention will be needed in order for the motions of the eye to obey Listing's law.

A second formulation of the equations of motion features Lagrange's equations of motion for the generalized coordinates ψ and θ. First, the kinetic energy $T = \frac{1}{2}\mathbf{J}\boldsymbol{\omega} \cdot \boldsymbol{\omega}$ of the rigid body is calculated with the help of (21). Expressed in a compact canonical form, it can be shown that

$$T = \frac{1}{2}m_{11}\dot{\theta}^2 + \frac{1}{2}m_{22}\dot{\psi}^2 + m_{12}\dot{\theta}\dot{\psi}, \tag{34}$$

where

$$\begin{aligned}
m_{11} &= \lambda_2 \cos^2(\psi) + \lambda_3 \sin^2(\psi), \\
m_{22} &= 4\lambda_1 \sin^4\left(\frac{\theta}{2}\right) + \left(\lambda_3 \cos^2(\psi) + \lambda_2 \sin^2(\psi)\right)\sin^2(\theta), \\
m_{12} &= (\lambda_3 - \lambda_2)\cos(\psi)\sin(\psi)\sin(\theta).
\end{aligned} \tag{35}$$

The resulting Lagrange's equations of motion are equivalent to the $\mathbf{w}_1$ and $\mathbf{w}_2$ components, respectively, of (33):

$$\frac{d}{dt}\left(\frac{\partial T}{\partial \dot{\theta}}\right) - \frac{\partial T}{\partial \theta} = 0, \qquad \frac{d}{dt}\left(\frac{\partial T}{\partial \dot{\psi}}\right) - \frac{\partial T}{\partial \psi} = 0, \tag{36}$$

The right-hand sides of (36) are zero because $\mathbf{M}_c \cdot \mathbf{w}_1 = \mathbf{M}_c \cdot \mathbf{w}_2 = 0$.

A third formulation of the equations of motion uses Hamilton's equations of motion. Starting from (34), the generalized momenta are

$$\begin{aligned}
p_\theta &= \frac{\partial T}{\partial \dot{\theta}} = m_{11}\dot{\theta} + m_{12}\dot{\psi}, \\
p_\psi &= \frac{\partial T}{\partial \dot{\psi}} = m_{12}\dot{\theta} + m_{22}\dot{\psi}.
\end{aligned} \tag{37}$$

---

[9] The prescription for the constraint moment is identical to Lagrange's prescription that is used in analytical dynamics (cf. [30]).

The Hamiltonian H can be computed from (34) and (37) using a Legendre transformation:

$$H = \frac{1}{2\left(m_{11}m_{22} - m_{12}^2\right)}\left(m_{22}p_\theta^2 + m_{11}p_\psi^2 - 2m_{12}p_\psi p_\theta\right).\tag{38}$$

The equations of motion for the eye are then found from Hamilton's equations of motion:

$$\dot{p}_\theta = -\frac{\partial H}{\partial \theta}, \qquad \dot{p}_\psi = -\frac{\partial H}{\partial \psi}, \qquad \dot{\theta} = \frac{\partial H}{\partial p_\theta}, \qquad \dot{\psi} = \frac{\partial H}{\partial p_\psi}.\tag{39}$$

These equations are equivalent to (36) and are convenient to use when examining how the dynamics of the system changes in response to changes in our assumptions on the mass moments of inertia λ_k. For instance if $\lambda_2 = \lambda_3$, then $m_{12} = 0$, $\frac{\partial H}{\partial \psi} = 0$, and, consequently, the momentum p_ψ will be conserved. The state space of the equations of motion (39) is four dimensional and visualizing the solutions can be difficult. In the sequel, we sometimes use the well-established practice of considering solutions to (39) corresponding to a fixed value of H. These solutions lie on a three-dimensional manifold in the four-dimensional state space. We can then construct a Poincaré section of this three-dimensional manifold and examine issues such as integrability and stability of periodic orbits.

The Lagrangian (36) and Hamiltonian (39) formulations is equivalent to (33) provided $\theta \neq 0$. When $\theta = 0$, the gaze direction is parallel to $\mathbf{E}_1$ and $\mathbf{R} = \mathbf{I}$. It is also appropriate to recall from Section 4.1 that when $\theta = 0$, $\mathbf{w}_2 = \mathbf{w}^3 = \mathbf{0}$ and hence $\left\{\mathbf{w}_1, \mathbf{w}_2, \mathbf{w}^3\right\}$ is not a basis for $\mathbb{E}^3$ when $\theta = 0$. Furthermore, the kinetic energy fails to be a positive-definite function of $\dot{\psi}$ and $\dot{\theta}$ when $\theta = 0$. This singularity manifests in our integrations of the equations of motion (36) (and their Hamiltonian counterparts (39)) near $\theta = 0$.

By non-dimensionalizing time using a constant frequency ω_0,

$$\tau = \omega_0 t,\tag{40}$$

we can non-dimensionalize the momenta and Hamiltonian:

$$\frac{\lambda_{2,3}}{\lambda_1}, \qquad \frac{p_\theta}{\lambda_1\omega_0}, \qquad \frac{p_\psi}{\lambda_1\omega_0}, \qquad \frac{H}{\lambda_1\omega_0^2}.\tag{41}$$

As ω_0 is arbitrary, for our numerical work in the sequel it will often suffice to consider cases where $H = 1$ and $\lambda_1 = 1$.

6.3 Geodesics

From analytical mechanics [39, Section 5.5] we know that the solutions to (36) not only conserve the energy T but they also constitute geodesics on the configuration manifold $\mathbb{RP}^2$ with respect to the kinematical line-element $ds = \sqrt{2T}\,dt$. Owing to the singularity in the coordinate system at $\theta = 0$, we need to supplement our analysis of (36) with an analysis of some of the solutions of (33) so as to capture other geodesics. To provide interpretation of the geodesics, we pay close attention to the path of $\mathbf{e}_1$ on the unit sphere. This curve traced by the tip of $\mathbf{e}_1$ is known as the spherical indicatrix. In particular, we (indirectly) classify the geodesics $\mathbb{RP}^2$ by the spherical indicatrix of $\mathbf{e}_1$.

As shall be apparent from the analysis in Section 7, when the eye is modeled as a symmetric rigid body, the corresponding solutions to (33) and (36) are geodesics of $SO(3)$ which satisfy Listing's constraint (25) and minimize the distance on $SO(3)$ between two configurations of the eye where the distance is measured using ds. The geodesics correspond to the motions where $\dot{\boldsymbol{\omega}} = \mathbf{0}$ and we are able to use [29] to add considerable detail to the preliminary remarks by Tweed *et al.* [40, p.106] and Hepp [14, p. 3239] and the geometric and numerical results in Ghosh *et al.* [7,8,31] on geodesics in the context of motions of the eye. When the eye is modeled as an axisymmetric or asymmetric rigid body, then some of the geodesics for the symmetric case are still present but new classes of geodesics also arise.

7 The Symmetric Case

The simplest conceivable model for the eye is to model it as a spherically symmetric rigid body: $\mathbf{J} = \lambda \mathbf{I}$. For this idealized case, there is a confluence of results from the literature on rotations and opthomalogy which enables us to trivially construct motions of the eye which satisfy the equations of motion (33). We find three classes of geodesics for this simple model and all three classes are easily interpreted.
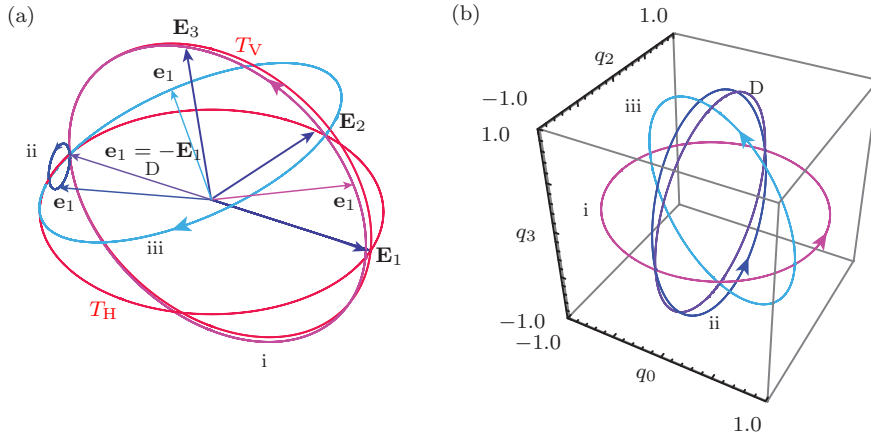
Fig. 8 *(a) Spherical indicatrices of the gaze direction* $\mathbf{e}_1$ *for the three classes of geodesic motions. The solutions labeled* T_H *is a Class I motion corresponding to a horizontal motion of the gaze direction, the solution labelled* T_V *is a Class I motion corresponding to a vertical motion of the gaze direction, the solutions labelled (i)-(iii) are Class II motions, and the solution labelled* D *is a Class III motion. (b) The quaternion components* (q_0, q_2, q_3) *corresponding to the periodic motions. The Class II and Class III solutions were obtained by integrating (43). For the cases shown:* $H = 1$, $\lambda_{1,2,3} = 1$, $\psi(0) = 0$, *and (i)* $\left(\theta(0) = \pi, p_\psi = 0.1\right)$, *(ii)* $\left(\theta(0) = \pi, p_\psi = 2.8\right)$, *(iii)* $\left(\theta(0) = \frac{7\pi}{4}, p_\psi = 1.08\right)$ *and (iv)* $(\theta(0) = \pi, p_\theta = 0.0)$.

7.1 Geodesics on the Configuration Manifold

For the case $\mathbf{J} = \lambda\mathbf{I}$, with the help of the expression (26) for $\dot{\boldsymbol{\omega}}$, a remarkable result was recently discovered by Cannata and Maggiali [2]: $\mathbf{M}_c = \mathbf{0}$ for the case where $\theta \neq 0$. In other words, for a perfectly symmetric eye, the muscles and soft tissues don't need to supply any torques for Listing's law to be enforced. In this case, the equations of motion simplify to

$$\dot{\boldsymbol{\omega}} = \mathbf{0}. \tag{42}$$

That is, the angular velocity vector of the eye is constant so we can appeal to the complete characterization of solutions to (42) which was recently published in O'Reilly and Payen [29]. These authors were unaware of Listing's law and the kinematics of the eye when they published their work.

7.1.1 Class I Motions of the Gaze Direction $\mathbf{e}_1$: The Great Circle Geodesics

To examine the geodesics of $SO(3)$ which satisfy Listing's law when $\mathbf{J} = \lambda\mathbf{I}$, we first use the equations of motion (33) restricted to the symmetric case, $\lambda\dot{\boldsymbol{\omega}} = \mathbf{M}_c$ and consider motions where $\dot{\boldsymbol{\omega}} = \mathbf{0}$. For this case, (33) implies that $\mathbf{M}_c = \mathbf{0}$. The trivial solutions to this case are those where $\boldsymbol{\omega}$ is constant and parallel to the axis of rotation: $\boldsymbol{\omega} = \dot{\theta}\mathbf{r}$ (i.e., $\ddot{\theta} = 0$ and $\dot{\mathbf{r}} = \mathbf{0}$). Because of Listing's law, $\mathbf{r}$ must lie in the $\mathbf{e}_2 - \mathbf{e}_3$ plane and hence $\mathbf{e}_1$ will trace out an arc of a great circle on the unit sphere. The great circle will pass through the occipital point Q (the point on the equator where $\mathbf{e}_1 = -\mathbf{E}_1$) as well as the primary point P (the point on the equator where $\mathbf{e}_1 = \mathbf{E}_1$). We call geodesics of this type Class I. It should be noted that for this class of geodesics it is possible for θ to range from 0 to 2π.

In the literature, two motions of the gaze direction of Class I are known as tertiary motions. Referring to Figure 8(a), these correspond to purely horizontal and purely vertical motions of the gaze direction and are respectively labelled T_{H} and T_{V} in this figure.

7.1.2 Class II and Class III Motions of the Gaze Direction $\mathbf{e}_1$

In addition to the Class I motions, other types of geodesics exist and these are most conveniently found from the Hamiltonian formulation of the equations of motion. For these motions $\dot{\boldsymbol{\omega}} = \mathbf{0}$ but the axis of rotation $\mathbf{r}$ is not parallel to $\boldsymbol{\omega}$ and $\mathbf{r}$ will describe a great circle as the motion evolves. Setting $\lambda_k = \lambda$ in (39) and rearranging, we find three differential equations of motion from which we can compute $\theta(t)$ and $\mathbf{r}(t)$:

$$\lambda\dot{\psi} = \frac{p_\psi}{1 - \cos{(\theta)}}, \qquad \dot{p}_\psi = 0, \qquad \lambda\ddot{\theta} - \frac{\sin{(\theta)}\,p_\psi^2}{\left(1 - \cos{(\theta)}\right)^2} = 0. \tag{43}$$

The solutions to these equations conserve the total energy E:

$$E = \frac{\lambda}{2}\dot{\theta}^2 + \frac{p_\psi^2}{1 - \cos{(\theta)}}. \tag{44}$$

As may be inferred from the phase portrait of (43)$_3$ shown in Figure 9, the differential equation (43)$_3$ has a fixed point at $\theta = \pi$ surrounded by closed periodic orbits. The singular behavior of the solutions to Hamilton's equations as $\theta \to 0$ should also be

noted from the phase portrait. Finally, we note that the coordinate ψ is ignorable and this will have consequences for the possible trajectories of $\mathbf{e}_1$ corresponding to solutions of (43).
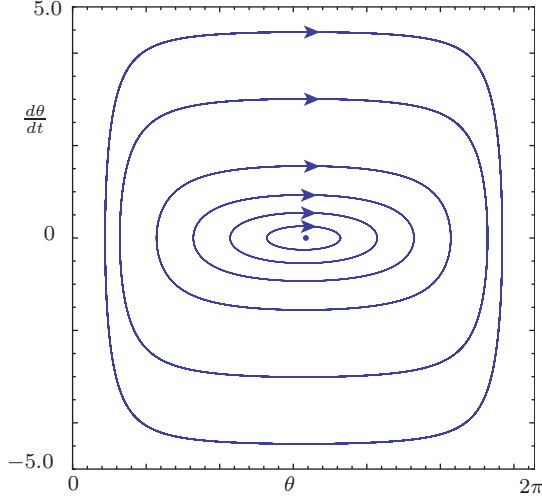
Fig. 9 *The phase portrait $\theta - \dot{\theta}$ of the differential equation $(43)_3$ corresponding to a constant value of $p_\psi = 1$ and $\lambda_{1,2,3} = 1$.*

The differential equations (43) are completely integrable and their solutions can be inferred from [29, Section 4] with minimal effort. In particular, we have the following analytical expressions for $\theta(t)$ and $\psi(t)$:

$$
\theta(t) = 2\cos^{-1}\left(c(t)\right), \qquad \psi(t) = \psi\left(t_0\right) + \operatorname{atan}\left(\frac{p_\psi}{\lambda\sqrt{2e_0}}\tan\left(f(t)\right)\right)\Bigg]_{t_0}^{t_1}, \qquad (45)
$$

where

$$
2e_0 = \boldsymbol{\omega}\left(t_0\right)\cdot\boldsymbol{\omega}\left(t_0\right),
$$

$$
c(t) = \pm\sqrt{1 - \frac{p_\psi^2}{2\lambda^2 e_0}}\sin\left(f(t)\right),
$$

$$
f(t) = \pm\frac{1}{2}\left(\sqrt{2e_0}\,t - \sqrt{2e_0}\,t_0\right) + \operatorname{atan}\left(\frac{\sqrt{2}\cos\left(\theta_0/2\right)}{\sqrt{1 - \frac{p_\psi^2}{\lambda^2 e_0}} - \cos\left(\theta_0\right)}\right). \qquad (46)
$$

It follows from (45) that the angular variables θ and ψ are periodic with a period $2T_g$:

$$
T_g = \frac{2\pi}{\|\boldsymbol{\omega}\|}. \qquad (47)
$$

It is of particular interest to note that $\theta(t)$ oscillates about π so, given a sufficient amount of time, motions of $\mathbf{e}_1$ are possible where $\mathbf{e}_1 = -\mathbf{E}_1$ for an instant. This

feature was noted previously by Ghosh and Wijayasinghe [7, Geodesic Theorem 2] and we will show that it is a consequence of a theorem by Helmholtz that is discussed in Section 7.2.[10]

To interpret the solutions (45) we consider a motion of the eye where the initial orientation is given by $\mathbf{e}_k(t_0)$ and the present orientation is prescribed by $\mathbf{e}_k(t)$. We can then define the rotation tensor $\mathbf{G}$ where

$$\mathbf{G}(t, t_0) = \mathbf{R}(t)\,\mathbf{R}^T(t_0), \qquad \mathbf{e}_k(t) = \mathbf{G}(t, t_0)\,\mathbf{e}_k(t_0). \tag{48}$$

For motions where $\boldsymbol{\omega}$ is constant, it was shown in [29] that the rotation $\mathbf{G}(t, t_0)$ corresponds to a rotation at a constant speed $\|\boldsymbol{\omega}(t_0)\|$ about the instantaneous axis of rotation $\mathbf{i} = \frac{\boldsymbol{\omega}(t_0)}{\|\boldsymbol{\omega}(t_0)\|}$. Although the axis $\mathbf{r}(t)$ of $\mathbf{R}(t)$ is generally varying with time, the instantaneous axis of rotation $\mathbf{i}$ is fixed. In addition, while $\mathbf{r}$ lies in all three planes $\mathcal{L}$, $\mathcal{F}$ and $\mathcal{V}$, $\mathbf{i}$ may only lie in the displacement plane $\mathcal{V}$.

Based on the results from [29] restricted to the case where the axis of rotation $\mathbf{r}$ lies in Listing's plane, we find two other classes of geodesics, which we denote by Class II and Class III. For completeness we also summarize our earlier classification of Class I geodesics.

I. The gaze direction traces out an arc of a great circle at constant speed. The circle passes through the primary position (where $\mathbf{e}_1 = \mathbf{E}_1$) and the occipital point Q (where $\mathbf{e}_1 = -\mathbf{E}_1$). The gaze direction can make a complete circuit in T_g seconds and $\boldsymbol{\omega} = \dot{\theta}\mathbf{r}$ lies on all three planes $\mathcal{V}$, $\mathcal{L}$, and $\mathcal{F}$.

II. The gaze direction traces out an arc of a circle centered about the constant angular velocity vector $\boldsymbol{\omega}$. The gaze direction can make a complete circuit in T_g seconds while the corresponding period of the axis of rotation $\mathbf{r}(t)$ is $2T_g$ seconds. During the cycle, the gaze direction will be parallel to $-\mathbf{E}_1$ for an instant. For these motions $\boldsymbol{\omega} = \dot{\theta}\mathbf{w}_1 + \dot{\psi}\mathbf{w}_2$.

III. The gaze direction is opposite the primary direction $\mathbf{e}_1 = -\mathbf{E}_1$ and points at the occipital point Q. The angle of rotation $\theta = \pi$ and, if p_ψ (or equivalently $\dot{\psi}$) is non-zero, then $\mathbf{e}_2$ and $\mathbf{e}_3$ will make a complete circuit in T_g seconds while the corresponding period of the axis of rotation $\mathbf{r}(t)$ will be $2T_g$ seconds. For this class of motions, $\boldsymbol{\omega} = \dot{\psi}\mathbf{w}_2$ and is normal to the axis of rotation $\mathbf{r} = \mathbf{w}_1$.

Examples of the indicatrices of $\mathbf{e}_1$ along with the corresponding traces of $q_0(t)$, $q_2(t)$ and $q_3(t)$ for all three classes of geodesics can be seen in Figure 8. As is apparent from this figure, the extreme versions of the Class II solutions asymptote to either a vertical rotation correspond to a Class I motion or a Class III motion.

7.2 The Geodesics in Relation to Helmholtz's Direction-Circles: Helmholtz's Theorem

In his treatise, Helmholtz [12, p. 79] defines certain spherical indicatrices of $\mathbf{e}_1$ which pass through the occipital point Q as *direction-circles*.[11] Based purely on a kinematical argument, he also establishes the following theorem which we paraphrase here and, following Hess [15], refer to as Helmholtz's theorem:

---

[10] Ghosh and Wijayasinghe [7] do not appear to have been aware of Helmholtz's theorem.

[11] We refer the interested reader to [36] for a discussion of how certain types of direction-circles were used by Helmholtz to analyze perception of straight lines in [12].

The prolongations of all circular paths described in turning around a fixed axis according to Listing's law will pass through Q. *Conversely, if the gaze direction obeying Listing's law describes an arc of a circle which passes through* Q *it must turn about a fixed axis which is normal to the plane of the given circle.*

Both of the fixed axis mentioned in this theorem correspond to the instantaneous axis of rotation, $\mathbf{i} = \frac{\boldsymbol{\omega}}{\|\boldsymbol{\omega}\|}$, and the Listing's law he refers to in the statement of the theorem is now known as Listing's half-angle rule. The spherical indicatrices of $\mathbf{e}_1$ which feature a constant $\mathbf{i}$ and pass through Q are defined as *direction-circles*.

While direction-circles are typically not great circles the same cannot be said for the locus of the unit vector $\mathbf{n}$ on the unit sphere. Because the unit vector $\mathbf{n} = \frac{\mathbf{w}^3}{\|\mathbf{w}^3\|}$ to the velocity plane $\mathcal{V}$ is always perpendicular to the vector $\boldsymbol{\omega}$ which passes through O, we find that the unit vector $\mathbf{n}$ will always trace out a great circle on a sphere centered at O when $\mathbf{e}_1$ traces out a circle. This fact was first noted by Helmholtz [12].

As can be seen from the results presented in Section 7.1, modeling the eye as a symmetric rigid body and analyzing the solutions to the equations of motion serves to prove Helmholtz' theorem in a manner that differs from the one found in [12, p. 79]. We note in particular the observation that for Class I motions $\boldsymbol{\omega} \parallel \mathbf{r} \parallel \mathbf{i}$ and so the fact that $\mathbf{e}_1$ can pass through Q follows trivially. For the Class II motions where $\mathbf{r}$ and $\mathbf{i}$ are distinct, the fact that $\mathbf{e}_1$ can pass through Q also follows trivially from the fixed point $\left(\theta, \dot{\theta}\right) = (\pi, 0)$ of $(43)_3$ (cf. Figure 9). An alternative proof that $\mathbf{e}_1$ passes through Q, which is also based on using a symmetric rigid body model for the eye, is presented in Ghosh and Wijayasinghe [7, Geodesic Theorem 2]. Later on in the present paper, when a non-symmetric model for the eye is examined, we find motions of the gaze direction which pass through Q for which the instantaneous axis $\mathbf{i}$ is not constant.

7.3 Constructing Geodesics Between Two Configurations of the Gaze Direction

A recent work by Hess [15] examined approximating saccades of rhesus monkeys using direction-circles. To do this, he approximated the saccades as a sequence of discrete fixed axis rotations and then determined the circular arcs for $\mathbf{e}_1(t)$ corresponding to the individual rotations. In other words, he exploiting the observation that given any two positions $\mathbf{e}_1(t_1)$ and $\mathbf{e}_1(t_2)$ of the gaze direction, the geodesics on $SO(3)$ that satisfies Listing's law when $\mathbf{J} = \lambda\mathbf{I}$ can be used to construct (iso-energetic) motions of $\mathbf{e}_1$ that will transit between $\mathbf{e}_1(t_1)$ and $\mathbf{e}_1(t_2)$. In principle, the number of possible paths to achieve this transit is limited only by the muscle innervation that will be needed to change the direction of motion of $\mathbf{e}_1$ at certain discrete events. In practice, given experimental data for $\mathbf{e}_1(t)$ and $\boldsymbol{\omega}(t)$, the actual path, number of discrete segments, and energy levels will be known.[12]

To elaborate, the Class I, II and III motions discussed earlier can be used to generate a coordinate system θ and ψ for the projective plane $\mathbb{RP}^2$ (cf. Figure 10). Consider the motion labelled T_V in Figure 8. This tertiary motion has an axis of rotation $\mathbf{r} = \mathbf{E}_2$ and is represented by the line $\psi = 0$ in the $\theta - \psi$ plane. By rotating the axis $\mathbf{r}$ through discrete increments of $\frac{\pi}{4}$ about $\mathbf{E}_1$ a series of great circles is generated by the spherical indicatrix of $\mathbf{e}_1$ corresponding to vertical lines in the $\theta - \psi$ plane (cf. Figure 10(a)&(b)). Similiarily for a Class II motion, such as the one labelled *iii* in Figure 8, by varying

---

[12] In Hess [15], only $\theta\mathbf{n} \cdot \mathbf{E}_k$ and $\mathbf{e}_1(t)$ are presented and so the energy level for each discrete component of the saccade is not given.
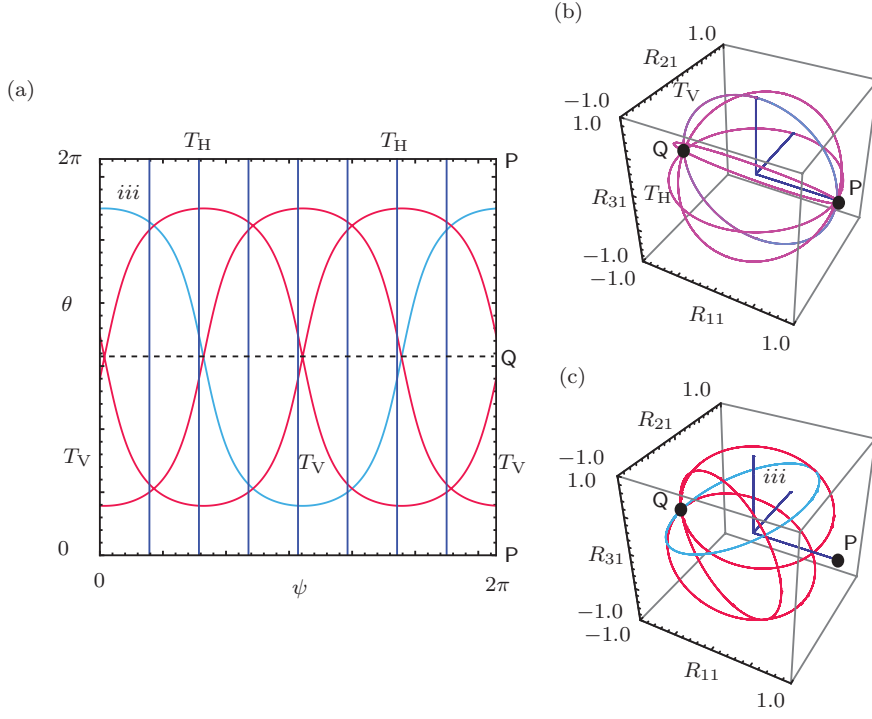
Fig. 10 *(a) Representations of Class I and Class II motions in the $\psi - \theta$ plane and the corresponding representations of the (b) Class I motions and (c) Class II motions as paths of the gaze direction. In these figures, the Class I motions are constructed by considering the motion T_V (cf. Figure 8) whose axis of rotation is $\mathbf{E}_2$ and phase shifting ψ in increments of $\frac{\pi}{4}$. Correspondingly the Class II motion is obtained by first considering the solution labelled iii (cf. Figure 8) and phase shifting the initial value of ψ in increments of $\frac{\pi}{2}$.*

the initial value of ψ in discrete increments of $\frac{\pi}{2}$, a set of three curves is generated in the $\theta - \psi$ plane. Each one of these three curves corresponds to a circular motion of $\mathbf{e}_1$ (cf. Figure 10(a)&(c)). We also observe that the process of varying the initial value of ψ by a discrete increment $\Delta\psi$ is equivalent to rotating the circle generated by the corresponding spherical indicatrix of $\mathbf{e}_1$ about $\mathbf{E}_1$ by an angle $\Delta\psi$.

Extrapolating from the above two examples, it should be clear that we can use Class I and Class II motions to generate a curvilinear coordinate system featuring θ and ψ for $\mathbb{RP}^2$. In addition to the fact that θ and ψ are 2π periodic, there are some unusual features of the coordinate system we are using for the plane. First, the occipital point Q is represented by a horizontal line $\theta = \pi$. Second, the principal point P is represented by the lines $\theta = 0$ and $\theta = 2\pi$. Finally, apart from P and Q, there is a two-to-one correspondence between points on this plane and the orientations of the gaze direction $\mathbf{e}_1$. That is,

$$(\theta, \psi) \equiv (2\pi - \theta, \psi + \pi). \tag{49}$$

The easiest example to observe this equivalence is to note the two copies of T_H in the $\theta - \psi$ plane in Figure 10(a).
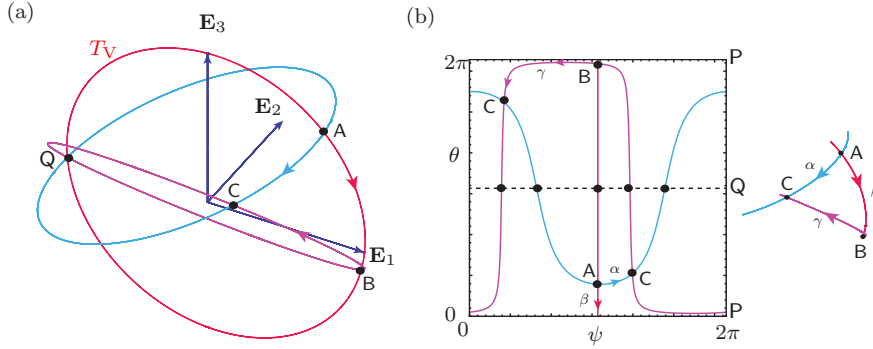
Fig. 11 *(a) Motion of the gaze direction from* A *to* C *along a Class II motion and the equivalent motion along a tertiary motion from* A *to* B *and a Class II motion* B *to* C *(b) Representation of the same motions (labelled α, and β and γ, respectively) on the projective plane* $\mathbb{RP}^2$ *parameterized by* θ *and* ψ. *On* $\mathbb{RP}^2$, *the occipital point* Q *and the principal point* P *are represented by horizontal lines and there is a two-to-one correspondence between points on this plane and the orientations of the gaze direction* $\mathbf{e}_1$.

To illustrate our comments, consider the motion of the gaze direction from A to C along the Class II motion shown in Figure 11. We can alternatively construct an equivalent motion along a Class I motion (which corresponds to the tertiary motion T_V from Figure 8) from A to B and then a motion from B to C along a Class II motion. It is easy to note that an infinite number of possible paths can be constructed. On each of the paths, the energy H can be identical to the original motion from A to C however at points such as B and A an angular impulse **L** must be provided to change the momentum. This impulse is related to the change in momentum by the following pair of jump conditions:

$$\llbracket p_\theta \rrbracket = \mathbf{L} \cdot \mathbf{w}_1, \qquad \llbracket p_\psi \rrbracket = \mathbf{L} \cdot \mathbf{w}_2. \tag{50}$$

Returning to our earlier discussion of Donders' law in Section 3, we also note that as a consequence of Listing's law, the net torsion about the gaze direction were $\mathbf{e}_1$ to describe the spherical triangle from A to B to C and back again to A would be zero. As astutely noted by Lamb [20, p. 688], in the absence of Listing's law one would expect the net torsion to be the area of the spherical triangle ABC which is non-zero (and in violation of Donders' law).

7.4 A Poincaré Section

The forthcoming cases, where $\mathbf{J} \neq \lambda \mathbf{I}$, cannot be classified as simply as we have just done. To see this it is useful to further elaborate on the solutions of (43). In particular, because the solutions to these equations of motion preserve p_ψ and H, we can construct a Poincaré section in the state space of (43) corresponding to a level set of $H = 1$, $\dot{\psi} > 0$ and $\psi > 0$. The Poincaré section is shown in Figure 12 and four samples of the solutions to (43) along with their corresponding gaze direction locii $\mathbf{e}_1(t)$ are also shown.

The Poincaré section shown in Figure 12 is indicative of an integrable system. Each periodic orbit of (43) appears as a single point on the Poincaré section. If we were to
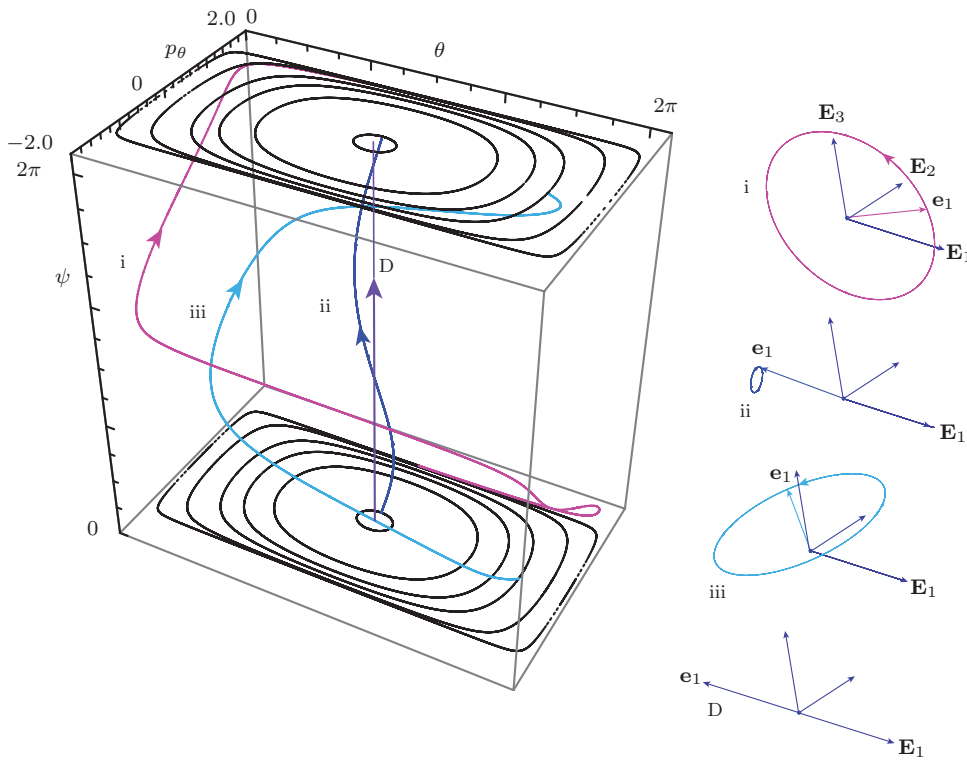
Fig. 12 *Four periodic motions in θ, ψ, p_θ space showing the Poincaré section $\psi = 0 \bmod (2\pi)$ for the differential equations (43). Three of these motions, which are labeled i-iii are Class II motions while the solution labeled D is a Class III motion. The inset images to the left of the Poincaré section show the spherical indicatrix of $\mathbf{e}_1$ corresponding to the trajectories. The parameter values and labeling of solutions (i)-(iii) and D is identical to the solutions shown in Figure 8.*

integrate (43) for all possible initial values of θ, p_ψ, and p_θ while keeping $H = 1$, then the Poincaré section shown in Figure 12 would resemble a solid round-edged rectangle. Indeed, the Poincaré map for this case is the identity mapping and every geodesic corresponds to a fixed point of the Poincaré map.

8 The Axisymmetric and Asymmetric Cases

When we remove the modeling assumption that $\mathbf{J} = \lambda\mathbf{I}$ the classification of the geodesics that we found in the symmetric case no longer holds. Indeed from all three classes of geodesics we can only prove that the Class I and III motions are present when in the axisymmetric case where $\lambda_2 = \lambda_3$ and, for the asymmetric case, only those two tertiary motions labeled T_H and T_V in Figure 13 are present. When the eye is assumed to be axisymmetric with $\lambda_2 = \lambda_3$, then we find that the equations of motion (39) are completely integrable, however the same cannot be said for the asymmetric case where

(a)   (b)
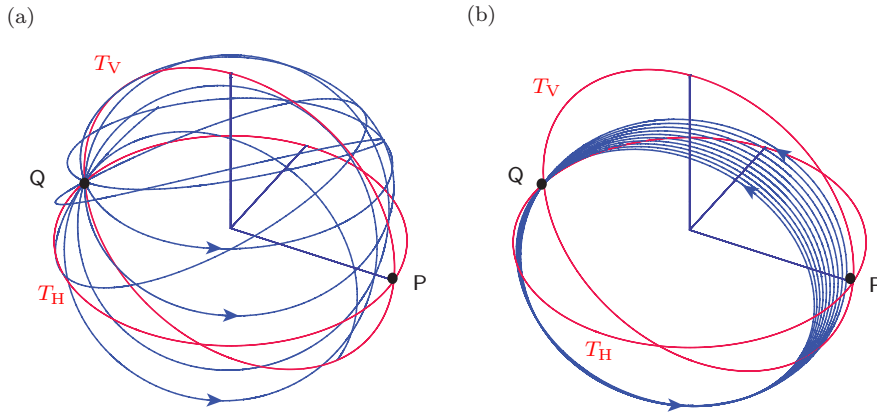
Fig. 13 *Three examples of the spherical indicatrices of the gaze direction* $\mathbf{e}_1$ *corresponding to the geodesics on* $\mathbb{RP}^2$ *for the (a) axisymmetric model and (b) asymmetric model of the eye. The solutions labeled* T_H *and* T_V *are Class I motions which correspond to geodesics in the* $\theta - \psi$ *projective plane* $\mathbb{RP}^2$. *For the other solutions, the moment of inertia values are identical to those used to construct Figures 14 and 16, respectively, and the initial conditions for the equations of motion (39) are* $\theta_0 = \pi$, $\psi_0 = 0$, $p_{\theta_0} = 0.0939715$, *and* $p_{\psi_0} = 1.08$.

the mass moments of inertia are distinct. In both the axisymmetric and asymmetric cases, for those geodesics on $\mathbb{RP}^2$ which don't correspond to constant values of ψ, the corresponding spherical indicatrices of $\mathbf{e}_1$ are no longer closed circles but instead are quasiperiodic motions which wind around the sphere. Two representative examples of these indicatrices are shown in Figure 13. For the asymmetric case, the complexity of the motion of $\mathbf{e}_1(t)$ was first noted in the recent paper by Ghosh *et al.* [8, Figure 8].

To elaborate on our previous comments, let us first examine the nature of the geodesics when $\mathbf{J} \neq \lambda \mathbf{I}$. We consider the equation of motion (33) and seek constant angular velocity solutions $\boldsymbol{\omega} = \boldsymbol{\omega}_0$ where $\dot{\boldsymbol{\omega}} = \mathbf{0}$ and $\mathbf{M}_c = \mathbf{0}$. In this case, (33) reduces to

$$\boldsymbol{\omega}_0 \times (\mathbf{J}\boldsymbol{\omega}_0) = \mathbf{0}. \tag{51}$$

This equation has a solution $\boldsymbol{\omega}_0$ which is parallel to an eigenvector of $\mathbf{J}$. For the axisymmetric case, any vector in the $\mathbf{e}_2 - \mathbf{e}_3$ plane is an eigenvector of $\mathbf{J}$, so $\boldsymbol{\omega}_0 = \omega_{0_2}\mathbf{e}_2 + \omega_{0_3}\mathbf{e}_3$. For such motions to be compatible with Listing's law, it is easy to show that $\mathbf{r}$ and $\boldsymbol{\omega}_0$ must be parallel:

$$\boldsymbol{\omega}_0 = \dot{\theta}_0\mathbf{r} \text{ where } \mathbf{r} = r_2\mathbf{e}_2 + r_3\mathbf{e}_3. \tag{52}$$

On the configuration manifold $\mathbb{RP}^2$, these solutions correspond to $\dot{\theta} = \dot{\theta}_0$ and $\psi = \psi_0$ and the resulting spherical indicatrices of $\mathbf{e}_1$ correspond to the Class I motions we defined earlier. For the asymmetric case, a parallel analysis of (51) leads to the conclusion that

$$\boldsymbol{\omega}_0 = \dot{\theta}_0\mathbf{E}_2 \text{ or } \boldsymbol{\omega}_0 = \dot{\theta}_0\mathbf{E}_3. \tag{53}$$

On $\mathbb{RP}^2$, these solutions correspond to $\dot{\theta} = \dot{\theta}_0$ and $\psi = 0$ or $\psi = \frac{\pi}{2}$ and the resulting spherical indicatrices of $\mathbf{e}_1$ correspond to the tertiary motions T_H and T_V in Figures 8 and 13.

(a)   (b)
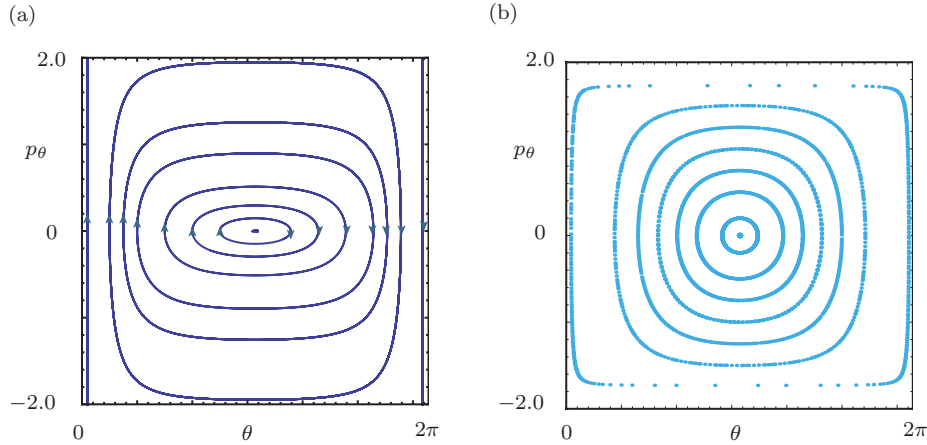
Fig. 14 *(a) The phase portrait of $\theta - p_\theta$ for a constant value of $p_\psi = 1$ for the differential equation $(54)_3$, and (b) the Poincaré map for the axisymmetric case that is obtained by integrating (54). For the numerical results shown, $\lambda_1 = 1.0$, $\lambda_2 = \lambda_3 = 1.50$, and $H = 1.0$ for the Poincaré map. The Poincaré section was constructed by sampling values of $p_\theta(t)$ and $\theta(t)$ corresponding to $\psi(t) = 0$ and $\dot{\psi}(t) > 0$.*

As regards integrability, if we consider the equations of motion (39) restricted to the case $\lambda_2 = \lambda_3$, then it is straightforward to show that both H and p_ψ are integrals of motion.[13] Indeed (39) simplify to

$$\lambda_1 \dot{\psi} = \frac{p_\psi}{4\lambda_1 \sin^4\left(\frac{\theta}{2}\right) + \lambda_3 \sin^2(\theta)},$$

$$\dot{p}_\psi = 0,$$

$$\lambda_3 \ddot{\theta} = \frac{((\lambda_3 - \lambda_1)\sin(2\theta) + 2\lambda_1 \sin(\theta)) p_\psi^2}{\left(4\lambda_1 \sin^2\left(\frac{\theta}{2}\right) + (\lambda_3 - \lambda_1)\sin^2(\theta)\right)^2}. \tag{54}$$

The equations of motion (54) can be integrated to provide analytical expressions for $\theta(t)$ and $\psi(t)$. However, in contrast to (45) the analytical expressions will feature hypergeometric functions and, in the interest of brevity, are not reproduced here. We can numerically integrate (54) to determine the phase portrait of $(54)_3$ and the resulting phase portrait is shown in Figure 14(a). The Poincaré map can also be constructed in an identical manner to the one shown in Figure 12. In contrast to the symmetric case, the resulting map has only one fixed point at $(\theta = \pi, p_\theta = 0)$. The fixed point of the Poincaré map corresponds to the Class III motion discussed in the symmetric case (see solution labelled D in Figures 8 and 12) The solutions $(\theta(t), \psi(t))$ define the geodesics on $\mathbb{RP}^2$ for this case.

For the axisymmetric model, the spherical indicatrices of $\mathbf{e}_1$ corresponding to geodesics no longer form closed circular curves but wind around the unit sphere. Because of the fixed point of (54) at $\theta = \pi$, the gaze direction has the potential to pass through the occipital point Q for all solutions of (54). Apart from the Class I motions, the instantaneous axis $\mathbf{i}$ is not constant as it was for the case considered in Section 7.2.

---

[13] I.e., ψ is an ignorable coordinate just as it was in the symmetric case.
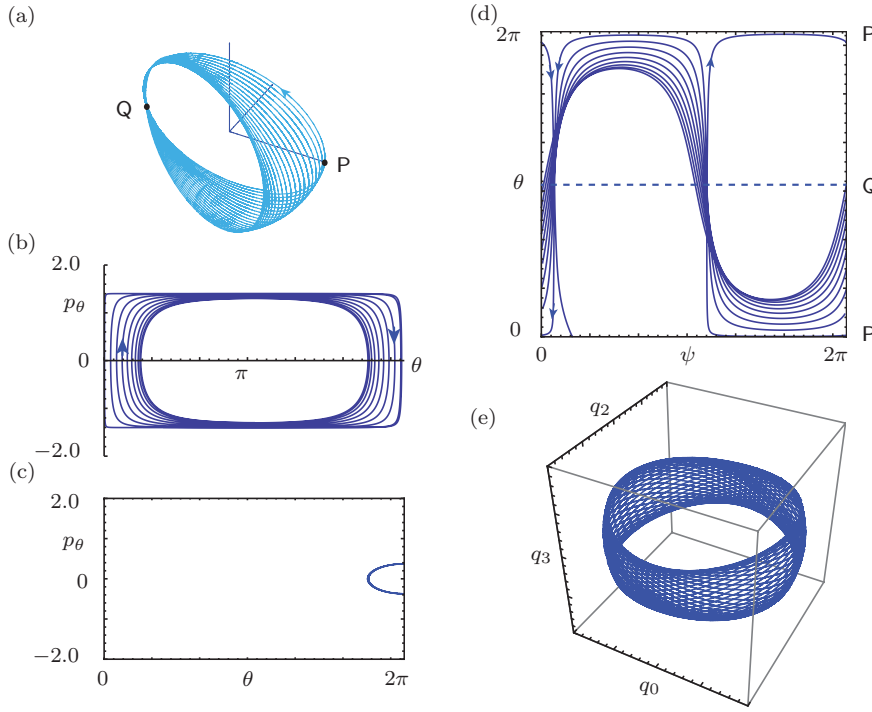
Fig. 15 *Features of a solution to the equations of motion for the asymmetric model. (a) Spherical indicatrix of the gaze direction $\mathbf{e}_1$, (b) phase portrait of the solution $(\theta(t), p_\theta(t))$ to (54), (c) Poincaré section of the solution $\big(\theta(t), \psi(t), p_\theta(t), p_\psi(t)\big)$ to (54), (d) the trajectory of $(\psi(t), \theta(t))$ on the $\psi - \theta$ plane, and (e) components of the unit quaternion $(q_0(t), q_2(t), q_3(t))$ computed using solutions $\theta(t)$ and $\psi(t)$ to (54). For the solution shown, $\lambda_1 = 1.0$, $\lambda_2 = 0.98$, $\lambda_3 = 1.02$, $H = 1.0$, $\psi(0) = 0.0$, $\theta(0) = \pi$, $p_\psi(0) = -1.04978\ldots$, and $p_\theta(0) = -1.3$*

For the asymmetric case, where $\mathbf{J}$ has distinct principal values, the equations of motion (39) no longer have an ignorable coordinate ψ and an associated conserved momentum p_ψ. Apart from the motions T_V and T_H, the spherical indicatrices of the gaze direction corresponding to the geodesic typically wind around the unit sphere. This feature can be seen in the representative example shown in Figure 15. For completeness, we have also indicated how the corresponding solution would appear on a phase portrait, Poincaré section, and $\psi - \theta$ plane. We also observe from Figure 15(e), that the behavior of (q_0, q_2, q_3) is far more complex than its symmetric counterpart shown in Figure 8(b). To examine the integrability of the canonical Hamiltonian system, we numerically constructed Poincaré maps. A representative example is shown in Figure 16. Observe from this figure that the equilibrium $(\theta = \pi, p_\theta = 0)$ has changed stability and that the behavior at $\theta = 0$ and $\theta = 2\pi$ has significant quantitative differences from its axisymmetric counterpart in Figure 14. We also find that as the λ_k became increasingly distinct, the Poincaré map displays an ever increasing number of stochastic zones (as we would expect from KAM theory).

For the axisymmetric and asymmetric models, we can still use the corresponding geodesics on $\mathbb{RP}^2$ to construct a framework for $\mathbf{e}_1$ as we did earlier in Section 7.3 for
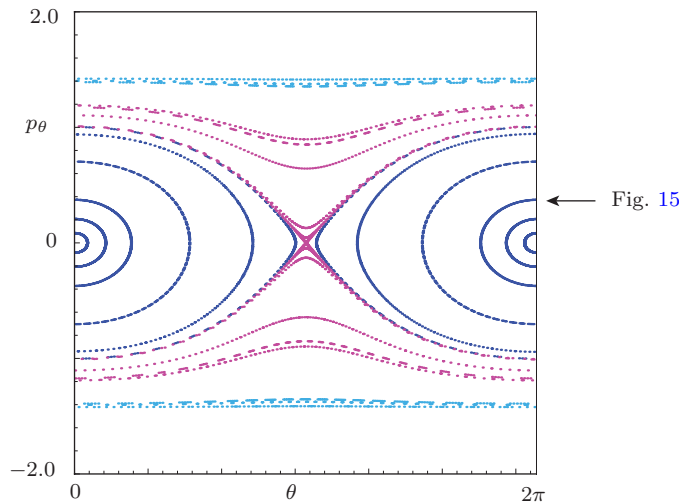
Fig. 16 *Poincaré map for the asymmetric eye obtained by integrating (39). For the numerical results shown, $\lambda_1 = 1.0$, $\lambda_2 = 0.98$, $\lambda_3 = 1.02$, and $H = 1.0$. The Poincaré section was constructed by sampling values of $p_\theta(t)$ and $\theta(t)$ corresponding to $\psi(t) = 0$ and $\dot{\psi}(t) > 0$. To facilitate comparisons to the literature, the values chosen for the mass moments of inertia are similar to those used in [8]. Multiple features of the solution labelled with the "←" are shown in Figure 15.*

the symmetric model. In this case the fact that the motions of $\mathbf{e}_1$ corresponding to geodesics no longer form simple closed circles can be exploited to generate paths of the gaze direction between any two points on the sphere. An example of such a situation can be seen in Figure 15(d).

It is of interest to reexamine Helmholtz's theorem that was discussed in Section 7.2. When the eye is modeled as non-symmetric rigid body, then, apart from the Class I geodesics for the axisymmetric case and the tertiary motions for the asymmetric case, the only way to have motions which correspond to the constant angular velocity motions his theorem describes is to impose an applied moment. For example, consider a constant angular velocity motion where $\boldsymbol{\omega} = \boldsymbol{\omega}_0$. Then, the balance of angular momentum can be used to show that an applied moment $\mathbf{M}_a$ must act in order for the eye to exhibit a constant angular velocity motion:

$$\mathbf{M}_a = -\mu \mathbf{n} + \boldsymbol{\omega}_0 \times (\mathbf{J}\boldsymbol{\omega}_0) . \tag{55}$$

In the absence of such an applied moment, the motions of the gaze direction found by integrating $\mathbf{J}\dot{\boldsymbol{\omega}} + \boldsymbol{\omega} \times (\mathbf{J}\boldsymbol{\omega}) = \mathbf{0}$ typically feature motions where $\dot{\boldsymbol{\omega}} \neq \mathbf{0}$ such as the two examples shown in Figure 13.

9 Concluding Comments

We have developed and analyzed a rigid-body based model for the dynamics of the eye. Even in the absence of muscles, the resulting dynamics exhibit a rich behavior and allow a remarkable range of motions for the gaze direction with minimal external intervention. For the symmetric eye and axisymmetric eye models, the wide spectrum

of motions can be partially attributed to the ignorable nature of the ψ coordinate, while for the asymmetric model, the spectrum of motions is provided by the quasiperiodic nature of the geodesics. It is also noteworthy that the range of motions persists even when the mass moments of inertia are varied and that all of the possible indicatrices of the gaze direction pass through the occipital point. To initiate these eye movements and to enable transition such as shown in Figure 11(b), the intervention of muscles are needed both at discrete events where the trajectory changes and to overcome viscous damping and the effects of the orbital tissues. We also note that while many of the motions of the gaze direction that we observed are not physiological it is important to construct a complete picture of the dynamics predicted by the simple models we examined so the more complex models featuring muscles can be more fully understood.

It is appropriate to comment on the work of Tweed *et al.* [40, p. 106]. They observed that the saccades found in their experiments were fixed axis of rotation motions and this inspired us to examine geodesics. In extrapolating our results to theirs, it is important to observe that fixed axis of rotation motions are only found in the symmetric model, for the Class I motions in the axisymmetric model, and for the tertiary motions T_V and T_H in the asymmetric models. Thus our qualitative results fail to capture the complexity of saccadic motions found by them (see, *e.g.,* [42, Figure 2]). To satisfactorily explain their results, it will be necessary to include models for the muscles and then proceed with a qualitative analysis of the resulting equations of motion. Such an analysis would complement the detailed state-of-the-art numerical model in [43].

In the context of rigid body dynamics, the non-integrability we observe in the asymmetric rigid body model for the eye is novel. Given the integrability of the equations of motion for the unconstrained rotational motion of an asymmetric rigid body, we would expect the corresponding holonomically constrained problem to be integrable, but this is not the case. Indeed the non-integrability has parallels to that for the case of an asymmetric body that is free to rotate about a fixed point O under the action of a gravitational force. This conservative mechanical system is non-integrable (cf. [21]).

Acknowledgements

References

1. Alexander, J.C., Antman, S.S.: The ambiguous twist of Love. Quarterly of Applied Mathematics **40**(1), 83–92 (1982/83)
2. Cannata, G., Maggiali, M.: Models for the design of bioinspired robot eyes. IEEE Transactions on Robotics **24**(1), 27–44 (2008). URL http://dx.doi.org/10.1109/TRO.2007.906270
3. Casey, J.: On the advantages of a geometrical viewpoint in the derivation of Lagrange's equations for a rigid continuum. In: J. Casey, M.J. Crochet (eds.) Theoretical, Experimental, and Numerical Contributions to the Mechanics of Fluids and Solids, pp. 805–847. Birkhaüser, Basel, Switzerland (1995). URL http://dx.doi.org/10.1007/978-3-0348-9229-2_41
4. Crawford, J.D., Vilis, T.: Axes of eye rotation and Listing's law during rotations of the head. Journal of Neurophysiology **65**(3), 407–423 (1991). URL http://jn.physiology.org/content/65/3/407

5. Demer, J., Oh, S., Clark, R., Poukens, V.: Evidence for a pulley of the inferior oblique muscle. Investigative Ophthalmology and Visual Science **44**(9), 3856–3865 (2003). URL http://dx.doi.org/10.1167/iovs.03-0160

6. Fetter, M., Haslwanter, T., Misslisch, H., Tweed, D. (eds.): Three-Dimensional Kinematics of Eye, Head and Limb Movements. Harwood Academic Publishers, Amsterdam, The Netherlands (1997)

7. Ghosh, B., Wijayasinghe, I.: Dynamics of human head and eye rotations under Donders' constraint. Automatic Control, IEEE Transactions on **57**(10), 2478–2489 (2012). URL http://dx.doi.org/10.1109/TAC.2012.2186183

8. Ghosh, B., Wijayasinghe, I., Kahagalage, S.: A geometric approach to head/eye control. Access, IEEE **2**, 316–322 (2014). URL http://dx.doi.org/10.1109/ACCESS.2014.2315523

9. Haslwanter, T.: Mathematics of three-dimensional eye rotations. Vision Research **35**(12), 1727–1739 (1995). URL http://dx.doi.org/10.1016/0042-6989(94)00257-M

10. van der Heijden, G.H.M., Peletier, M.A., Planqué, R.: On end rotation for open rods undergoing large deformations. Quarterly of Applied Mathematics **65**(2), 385–402 (2007). URL http://dx.doi.org/10.1090/S0033-569X-07-01049-X

11. Helmholtz, H.: Ueber die normalen Bewegungen des menschlichen Auges. Archiv für Ophthalmologie **9**(2), 153–214 (1863). URL http://dx.doi.org/10.1007/BF02720895

12. von Helmholtz, H.: A Treatise on Physiological Optics, vol. III. Dover Publications, New York (1962). Translated from the (1910) third German edition and edited by J.P.C. Southall

13. Hepp, K.: On Listing's law. Communications in Mathematical Physics **132**(1), 285–292 (1990). URL http://dx.doi.org/10.1007/BF02278012

14. Hepp, K.: Theoretical explanations of Listing's law and their implication for binocular vision. Vision Research **35**(23–24), 3237–3241 (1995). URL http://dx.doi.org/10.1016/0042-6989(95)00104-M

15. Hess B, J.M.: Three-dimensional visuo-motor control of saccades. Journal of Neurophysiology **109**(1), 183–192 (2012). URL http://dx.doi.org/10.1152/jn.00513.2012

16. Hestenes, D.: Invariant body kinematics: I. Saccadic and compensatory eye movements. Neural Networks **7**(1), 65–77 (1994). URL http://dx.doi.org/10.1016/0893-6080(94)90056-6

17. Howard, I.P., Evans, J.A.: The measurement of eye torsion. Vision Research **3**(9–10), 447–455 (1963). URL http://dx.doi.org/10.1016/0042-6989(63)90095-6

18. Judge, S.J.: Reflection makes sense of rotation of the eyes. Vision Research **46**(22), 3862–3866 (2006). URL http://dx.doi.org/10.1016/j.visres.2006.05.006

19. Kushner, B.J.: Ocular torsion: Rotations around the "Why" axis. Journal of American Association for Pediatric Ophthalmology and Strabismus **8**(1), 1–12 (2004). URL http://dx.doi.org/10.1016/j.jaapos.2003.09.004

20. Lamb, H.: The kinematics of the eye. Philosophical Magazine Series 6 **38**(228), 685–695 (1919). URL http://dx.doi.org/10.1080/14786441208636001

21. Lewis, D., Ratiu, T., Simo, J.C., Marsden, J.E.: The heavy top: A geometric treatment. Nonlinearity **5**(1), 1–48 (1992). URL http://dx.doi.org/10.1088/0951-7715/5/1/001

22. Liversedge, S.P., Gilchrist, I.D., Everling, S. (eds.): The Oxford Handbook of Eye Movements. Oxford University Press, Oxford, New York (2011)

23. Love, A.E.H.: A Treatise on the Mathematical Theory of Elasticity. Dover Publications, Inc., New York (1944)

24. Miller, J.M.: Understanding and misunderstanding extraocular muscle pulleys. Journal of Vision **7**(11) (2007). URL http://dx.doi.org/10.1167/7.11.10

25. Miller, J.M., Robinson, D.A.: A model of the mechanics of binocular alignment. Computers and Biomedical Research **17**(5), 436–470 (1984). URL http://dx.doi.org/10.1016/0010-4809(84)90012-0

26. Nakayama, K.: Kinematics of normal and strabismic eyes. In: C.M. Schur, K.J. Ciuffreda (eds.) Vergence Eye Movements: Basic and Clinical Aspects, chap. 16, pp. 543–564. Butterworths, Boston, MA (1983)

27. O'Reilly, O.M.: On the computation of relative rotations and geometric phases in the motions of rigid bodies. ASME Journal of Applied Mechanics **64**(4), 969–974 (1997). URL http://dx.doi.org/10.1115/1.2789008

28. O'Reilly, O.M.: Intermediate Dynamics for Engineers: A Unified Treatment of Newton-Euler and Lagrangian Mechanics. Cambridge University Press, Cambridge (2008)

29. O'Reilly, O.M., Payen, S.: The attitudes of constant angular velocity motions. Internat. J. Non-Linear Mech. **41**(6–7), 1–10 (2006). URL http://dx.doi.org/10.1016/j.ijnonlinmec.2006.05.001

30. O'Reilly, O.M., Srinivasa, A.R.: A simple treatment of constraint forces and constraint moments in the dynamics of rigid bodies. ASME Applied Mechanics Reviews **67**(1), 014,801 (2014). URL http://dx.doi.org/10.1115/1.4028099

31. Polpitiya, A., Dayawansa, W., Martin, C., Ghosh, B.: Geometry and control of human eye movements. IEEE Transactions on Automatic Control **52**(2), 170–180 (2007). URL http://dx.doi.org/10.1109/TAC.2006.887902

32. Quaia, C., Optician, L.M.: Three-dimensional rotations of the eye. In: L.A. Levin (ed.) Adler's Physiology of the Eye, eleventh edn., pp. 208–219. Elsevier, New York (2011)

33. Raphan, T.: Modeling control of eye orientation in three dimensions. I. Role of muscle pulleys in determining saccadic trajectory. Journal of Neurophysiology **79**(5), 2653–2667 (1998). URL http://jn.physiology.org/content/79/5/2653.abstract

34. Robinson, D.: A method of measuring eye movement using a scieral search coil in a magnetic field. Bio-medical Electronics, IEEE Transactions on **10**(4), 137–145 (1963). URL http://dx.doi.org/10.1109/TBMEL.1963.4322822

35. Robinson, D.: A quantitative analysis of extraocular muscle corporation and squint. Investigative Opthalmology and Vision Science **14**(11), 801–825 (1975)

36. Rogers, B., Brecher, K.: Straight lines, 'uncured lines', and Helmholtz's 'great circles on the celestial sphere'. Perception **36**(9), 1275–1289 (2007). URL http://dx.doi.org/10.1068/p5652

37. Schreiber, K.M., Schor, C.M.: A virtual ophthalmotrope illustrating oculomotor coordinate systems and retinal projection geometry. Journal of Vision **7**(10), 1–14 (2007). URL http://dx.doi.org/10.1167/7.10.4

38. Simonsz, H.J., Tonkelaar, I.: 19th Century mechanical models of eye movements, Donders' law, Listing's law and Helmholtz' direction circles. Documenta Ophthalmologica **74**(1–2), 95–112 (1990). URL http://dx.doi.org/10.1007/BF00165667

39. Synge, J.L., Schild, A.: Tensor Calculus. University of Toronto Press, Toronto (1949)

40. Tweed, D., Cadera, W., Vilis, T.: Computing three-dimensional eye position quaternions and eye velocity from search coil signals. Vision Research **30**(1), 97–110 (1990). URL http://dx.doi.org/10.1016/0042-6989(90)90130-D

41. Tweed, D., Vilis, T.: Implications of rotational kinematics for the oculomotor system in three dimensions. Journal of Neurophysiology **58**(4), 832–849 (1987)

42. Tweed, D., Vilis, T.: Geometric relations of eye position and velocity vectors during saccades. Vision Research **30**(1), 111–127 (1990). URL http://dx.doi.org/10.1016/0042-6989(90)90131-4

43. Wei, Q., Sueda, S., Pai, D.K.: Physically-based modeling and simulation of extraocular muscles. Progress in Biophysics and Molecular Biology **103**(2/3), 273–283 (2010). URL http://dx.doi.org/10.1016/j.pbiomolbio.2010.09.002. Special Issue on Biomechanical Modelling of Soft Tissue Motion

44. Westheimer, G.: Kinematics of the eye. Journal of the Optical Society of America **47**(10), 967–974 (1957). URL http://dx.doi.org/10.1364/JOSA.47.000967

45. Wong, A.M.F.: Listing's law: Clinical significance and implications for neural control. Survey of Ophthalmology **49**(6), 563–575 (2004). URL http://dx.doi.org/10.1016/j.survophthal.2004.08.002

A Background on Rotations

In the present paper, a tensor notation for the rotation is employed following [3, 28]. This notation enables us to easily establish the identity that leads to additional insight into Listing's law. All vectors in Euclidean three-space $\mathbb{E}^3$ are denoted by bold-faced letters. A tensor can be considered as a linear operator which transforms a vector in $\mathbb{E}^3$ to another vector in $\mathbb{E}^3$. For example, $\mathbf{a} \otimes \mathbf{b}$ transforms $\mathbf{c}$ to the vector $(\mathbf{b} \cdot \mathbf{c}) \mathbf{a}$: $(\mathbf{a} \otimes \mathbf{b}) \mathbf{c} = (\mathbf{b} \cdot \mathbf{c}) \mathbf{a}$.

We start with a set of fixed right-handed basis vectors $\{\mathbf{E}_1, \mathbf{E}_2, \mathbf{E}_3\}$. The rotation tensor $\mathbf{R}$ transforms each of the basis vectors $\mathbf{E}_i$ into a vector $\mathbf{e}_i$: $\mathbf{R}\mathbf{E}_i = \mathbf{e}_i$. Because $\mathbf{R}$ is a rotation it can be shown that $\{\mathbf{e}_1, \mathbf{e}_2, \mathbf{e}_3\}$ is a right-handed orthonormal basis. This basis is called the corotational basis because it corotates with a rigid body model for the eye.

To specify a rotation it suffices to prescribe an axis of rotation and an angle of rotation θ. The axis of rotation can be defined using a unit vector $\mathbf{r}$. Alternatively, the rotation tensor can be prescribed by a quaternion $(q_0, \mathbf{q})$ where q_0 is a scalar and $\mathbf{q}$ is a vector. Here, these 4 parameters satisfy the Euler parameter constraint $q = 1$ where $q = q_0^2 + \mathbf{q} \cdot \mathbf{q}$ and the

quaternion is known as a unit quaternion. A third alternative parameterization is to use a set of Euler angles. There are 12 possible choices of Euler angles and the literature on the kinematics of the eye is dominated by two of them. In studies on the kinematics of the eye, all of the aforementioned parameterizations have been used to successful explore features of the kinematics.

In what follows, we collect necessary background material on rotations from a range of sources and present it in a unified manner. Because of the widespread differences in how Euler angles are defined in the literature, we note explicitly here that our treatment of Euler angles follows that presented in the textbook [28]. Before addressing Euler angles, we find it convenient to start our discussion of the representation for a rotation tensor by using the quaternion representation. Using this representation to study the kinematics of the eye was championed by Westheimer [44] and, more recently, was successfully used by Tweed, Vilis, and their coworkers [4, 40, 41, 42].

A.1 The Rotation Tensor and its Components

The parameters q_0 and $\mathbf{q}$ of a unit quaternion can be used to define a rotation about an axis $\mathbf{r}$ through an angle θ using the identifications

$$q_0 = \cos\left(\frac{\theta}{2}\right), \quad \mathbf{q} = \sin\left(\frac{\theta}{2}\right)\mathbf{r}. \tag{A.1}$$

The resulting representation of the rotation tensor $\mathbf{R}$ is

$$\mathbf{R} = \mathbf{R}\left(q_0, \mathbf{q}\right) = \left(q_0^2 - \mathbf{q} \cdot \mathbf{q}\right)\mathbf{I} + 2\mathbf{q} \otimes \mathbf{q} + 2q_0 \text{ skewt}\left(\mathbf{q}\right). \tag{A.2}$$

In this representation, the skew-symmetric tensor of $\mathbf{a}$, skewt $(\mathbf{a})$, is a skew-symmetric tensor with the property that skewt $(\mathbf{a})\mathbf{b} = \mathbf{a} \times \mathbf{b}$ for all vectors $\mathbf{a}$ and $\mathbf{b}$.

As $\mathbf{R}$ transforms $\mathbf{E}_k$ to a vector $\mathbf{e}_k$: $\mathbf{R}\mathbf{E}_k = \mathbf{e}_k$ where $k = 1, 2, 3$, it can be shown that $\mathbf{R} = \sum_{i=1}^{3} \mathbf{e}_i \otimes \mathbf{E}_i = \sum_{i=1}^{3}\sum_{k=1}^{3} R_{ik}\mathbf{e}_i \otimes \mathbf{e}_k = \sum_{i=1}^{3}\sum_{k=1}^{3} R_{ik}\mathbf{E}_i \otimes \mathbf{E}_k$. Here, R_{ik} are known as the components of $\mathbf{R}$.

We note the important property that the axis of rotation remains unchanged by the rotation:

$$\mathbf{R}\mathbf{r} = \mathbf{r}, \tag{A.3}$$

and hence $\mathbf{R}^T\mathbf{R}\mathbf{r} = \mathbf{R}^T\mathbf{r}$. Because $\mathbf{R}^T\mathbf{R} = \mathbf{I}$ where $\mathbf{I}$ is the identity tensor, $\mathbf{r}$ is also unchanged by the inverse of the rotation:

$$\mathbf{r} = \mathbf{R}^T\mathbf{r}. \tag{A.4}$$

It is now straightforward to show using the identity $\mathbf{a} \cdot \mathbf{e}_k = \mathbf{a} \cdot (\mathbf{R}\mathbf{E}_k) = \left(\mathbf{R}^T\mathbf{a}\right) \cdot \mathbf{E}_k$ that, for all vectors $\mathbf{a}$,

$$r_k = \mathbf{r} \cdot \mathbf{e}_k = \mathbf{r} \cdot \mathbf{E}_k, \qquad q_k = \mathbf{q} \cdot \mathbf{e}_k = \mathbf{q} \cdot \mathbf{E}_k. \tag{A.5}$$

This common feature of the vectors $\mathbf{r}$ and $\mathbf{q}$, namely that they have the same components in the fixed and corotational bases, will be the source of many of our observations on Listing's law.

Examining the components $R_{ik} = \mathbf{e}_k \cdot \mathbf{E}_i$ of the tensor $\mathbf{R}$ one finds that

$$\mathsf{R} = \begin{bmatrix} R_{11} & R_{12} & R_{13} \\ R_{21} & R_{22} & R_{23} \\ R_{31} & R_{32} & R_{33} \end{bmatrix} = \left(2q_0^2 - 1\right)\begin{bmatrix} 1 & 0 & 0 \\ 0 & 1 & 0 \\ 0 & 0 & 1 \end{bmatrix} + 2\begin{bmatrix} q_1^2 & q_1 q_2 & q_1 q_3 \\ q_1 q_2 & q_2^2 & q_2 q_3 \\ q_1 q_3 & q_2 q_3 & q_3^2 \end{bmatrix} + 2q_0\begin{bmatrix} 0 & -q_3 & q_2 \\ q_3 & 0 & -q_1 \\ -q_2 & q_1 & 0 \end{bmatrix}. \tag{A.6}$$

The column vectors of the matrix R define the components of the moving bases vectors relative to their fixed counterparts and vice versa:

$$\mathbf{e}_k = R_{1k}\mathbf{E}_1 + R_{2k}\mathbf{E}_2 + R_{3k}\mathbf{E}_3, \qquad \mathbf{E}_k = R_{k1}\mathbf{e}_1 + R_{k2}\mathbf{e}_2 + R_{k3}\mathbf{e}_3. \tag{A.7}$$

These identities enable us to later construct $\mathbf{e}_i(t)$ given q_0 and $\mathbf{q}$.

A.2 Euler Angle Parameterizations

In many studies of the ocular system, several sets from the 12 possible sets of Euler angles are used to parameterize the rotation tensor $\mathbf{R}$. For instance, Fick in 1854 is credited with using a 3-2-1 set of Euler angles [9, 26, 37] to examine the kinematics of the eye having a gaze direction $\mathbf{e}_1$. This set of angles, which are sometimes known as "Fick coordinates," also feature in the classic work by Helmholtz [11, p.207] from 1865. Later, in his highly influential treatise [12], Helmholtz uses both a 2-3-1 set of Euler angles (cf. [12, pp. 43–44]) and a set of 1-3-1 Euler angles (cf. [12, pp. 73–75]). The 2-3-1 set of Euler angles is sometimes known as "Helmholtz coordinates" (cf. [37]).

In principle it is possible to use any of the 12 sets of Euler angles to parameterize $\mathbf{R}$. However, depending on the issue of interest, asymmetric sets such as the 3-2-1 set have advantages over the symmetric sets, such as the 1-2-1. Indeed, we find it convenient to consider both a 3-2-1 and a 1-2-1 set of Euler angles. The 1-2-1 set is advantageous both as a means to compare with the quaternion parameterization of the eye's rotation and as a transparent representation of Listing's law. By way of contrast, while the 3-2-1 set provides the most transparent measure of the angle of (ocular) torsion and a treatment of Donders' law, the 3-2-1 set produces an unwieldy representation of Listing's law.

A.2.1 A 1-2-1 Euler angle parameterization

For the 1-2-1 parameterization, we first rotate about $\mathbf{E}_1$ through a counterclockwise angle of rotation θ_1, then we rotate about $\mathbf{e}_2' = \cos{(\theta_1)}\,\mathbf{E}_2 - \sin{(\theta_1)}\,\mathbf{E}_3$ through a counterclockwise angle θ_2, and finally we rotate about $\mathbf{e}_1$ through a counterclockwise angle of rotation θ_3:

$$\mathbf{e}_1 = \cos{(\theta_2)}\,\mathbf{E}_1 + \sin{(\theta_2)}\sin{(\theta_1)}\,\mathbf{E}_2 - \sin{(\theta_2)}\cos{(\theta_1)}\,\mathbf{E}_3. \tag{A.8}$$

To show the equivalence of the Euler angle parameterization to the earlier quaternion based parameterization, we use known formulae from quaternion algebra for the composition of rotations (see, e.g., [28, p. 201]. After a substantial amount of algebra it can be concluded that

$$q_0 = \cos\left(\frac{\theta_2}{2}\right)\cos\left(\frac{\theta_1}{2} + \frac{\theta_3}{2}\right),$$
$$q_1 = \cos\left(\frac{\theta_2}{2}\right)\sin\left(\frac{\theta_1}{2} + \frac{\theta_3}{2}\right),$$
$$q_2 = \sin\left(\frac{\theta_2}{2}\right)\cos\left(\frac{\theta_1}{2} - \frac{\theta_3}{2}\right),$$
$$q_3 = \sin\left(\frac{\theta_2}{2}\right)\sin\left(\frac{\theta_1}{2} - \frac{\theta_3}{2}\right). \tag{A.9}$$

These expressions are used to demonstrate equivalent formulations of Listing's law. We can also express the components of $\mathbf{R}$ in terms of the 1-2-1 set of Euler angles. The resulting lengthy expressions are omitted in the interests of brevity.

A.2.2 A 3-2-1 Euler angle parameterization

The second set of Euler angles that prominently features in the discussions of the ocular system is the 3-2-1 set. As mentioned earlier, use of this set dates to Fick in the 1850s and, as noted by [37], the 3-2-1 set is the easiest set to use when trying to understanding the motion of the gaze direction. When using a set of 3-2-1 Euler angles to parameterize of the rotation of the eye, we first rotate about $\mathbf{E}_3$ through a counterclockwise angle of rotation ϕ_1, then we rotate about $\mathbf{e}_2' = \cos{(\phi_1)}\,\mathbf{E}_2 + \sin{(\phi_1)}\,\mathbf{E}_1$ through a counterclockwise angle ϕ_2, and finally we rotate about $\mathbf{e}_1$ through a counterclockwise angle of rotation ϕ_3:

$$\mathbf{e}_1 = \cos{(\phi_1)}\cos{(\phi_2)}\,\mathbf{E}_1 + \sin{(\phi_1)}\cos{(\phi_2)}\,\mathbf{E}_2 - \sin{(\phi_2)}\,\mathbf{E}_3. \tag{A.10}$$

The angle ϕ_3 in this parameterization can be used to measure ocular torsion (or the rolling motion of the eye), but this measurement is easily prone to misinterpretation.

Omitting details, we find that corresponding expressions for the components of the quaternion $(q_0, \mathbf{q})$ that is used to parameterize the same rotation $\mathbf{R}$ as the set of 3-2-1 Euler angles are

$$q_0 = \cos\left(\frac{\phi_1}{2}\right)\cos\left(\frac{\phi_2}{2}\right)\cos\left(\frac{\phi_3}{2}\right) + \sin\left(\frac{\phi_1}{2}\right)\sin\left(\frac{\phi_2}{2}\right)\sin\left(\frac{\phi_3}{2}\right),$$

$$q_1 = \cos\left(\frac{\phi_1}{2}\right)\cos\left(\frac{\phi_2}{2}\right)\sin\left(\frac{\phi_3}{2}\right) - \sin\left(\frac{\phi_1}{2}\right)\sin\left(\frac{\phi_2}{2}\right)\cos\left(\frac{\phi_3}{2}\right),$$

$$q_2 = \cos\left(\frac{\phi_1}{2}\right)\sin\left(\frac{\phi_2}{2}\right)\cos\left(\frac{\phi_3}{2}\right) + \sin\left(\frac{\phi_1}{2}\right)\cos\left(\frac{\phi_2}{2}\right)\sin\left(\frac{\phi_3}{2}\right),$$

$$q_3 = \sin\left(\frac{\phi_1}{2}\right)\cos\left(\frac{\phi_2}{2}\right)\cos\left(\frac{\phi_3}{2}\right) - \cos\left(\frac{\phi_1}{2}\right)\sin\left(\frac{\phi_2}{2}\right)\sin\left(\frac{\phi_3}{2}\right). \tag{A.11}$$

Again, in the interests of brevity, we do not provide explicit expressions for the components of $\mathbf{R}$ in terms of the Euler angles.

A.3 Angular Velocity Vectors

The angular velocity vector $\boldsymbol{\omega}$ associated with the rotation tensor $\mathbf{R}$ is defined as the axial vector of the skew-symmetric tensor $\dot{\mathbf{R}}\mathbf{R}^T$: $\mathrm{skewt}\left(\boldsymbol{\omega}\right)\mathbf{a} = \dot{\mathbf{R}}\mathbf{R}^T\mathbf{a}$ for all vectors $\mathbf{a}$. Differentiating the identity $\mathbf{e}_k = \mathbf{R}\mathbf{E}_k$ with respect to time t, it can be shown that

$$\dot{\mathbf{e}}_k = \boldsymbol{\omega} \times \mathbf{e}_k. \tag{A.12}$$

It can also be shown that $\boldsymbol{\omega}$ has the representation[14]

$$\boldsymbol{\omega} = 2\left(q_0\dot{\mathbf{q}} - \dot{q}_0\mathbf{q} + \mathbf{q} \times \dot{\mathbf{q}}\right). \tag{A.13}$$

The corresponding representations for $\boldsymbol{\omega}$ in terms of the 1-2-1 and 3-2-1 sets of Euler angles are easily written down[15] but are omitted here in the interests of brevity.

Taking the $\mathbf{E}_i$ and $\mathbf{e}_k$ components of $\boldsymbol{\omega}$ given by (A.13) leads to the results

$$\begin{bmatrix} \boldsymbol{\omega} \cdot \mathbf{E}_1 \\ \boldsymbol{\omega} \cdot \mathbf{E}_2 \\ \boldsymbol{\omega} \cdot \mathbf{E}_3 \end{bmatrix} = \mathsf{A}\begin{bmatrix} \dot{q}_0 \\ \dot{q}_1 \\ \dot{q}_2 \\ \dot{q}_3 \end{bmatrix}, \qquad \begin{bmatrix} \boldsymbol{\omega} \cdot \mathbf{e}_1 \\ \boldsymbol{\omega} \cdot \mathbf{e}_2 \\ \boldsymbol{\omega} \cdot \mathbf{e}_3 \end{bmatrix} = \mathsf{C}\begin{bmatrix} \dot{q}_0 \\ \dot{q}_1 \\ \dot{q}_2 \\ \dot{q}_3 \end{bmatrix}, \tag{A.14}$$

where

$$\mathsf{A} = 2\begin{bmatrix} -q_1 & q_0 & -q_3 & q_2 \\ -q_2 & q_3 & q_0 & -q_1 \\ -q_3 & -q_2 & q_1 & q_0 \end{bmatrix}, \qquad \mathsf{C} = 2\begin{bmatrix} -q_1 & q_0 & q_3 & -q_2 \\ -q_2 & -q_3 & q_0 & q_1 \\ -q_3 & q_2 & -q_1 & q_0 \end{bmatrix}. \tag{A.15}$$

A compact expression for the angular acceleration components $\dot{\boldsymbol{\omega}} \cdot \mathbf{E}_k$ as a product of A and the array $[\ddot{q}_0, \ddot{q}_1, \ddot{q}_2, \ddot{q}_3]^T$ can be easily deduced from (A.13) and (A.14)$_1$.

---

[14] See, e.g., [28, Sect. 6.9].
[15] See, e.g., [28, Sect. 6.8].